GENERATION OF SURFACE WAVES DUE TO SUDDEN MOVEMENTS AT THE SEA BOTTOM

A THESIS SUBMITTED TO
THE GRADUATE SCHOOL OF NATURAL AND APPLIED SCIENCES
OF
THE MIDDLE EAST TECHNICAL UNIVERSITY

BY

ÖZGÜR ULAŞ KIRLANGIÇ

IN PARTIAL FULFILLMENT OF THE REQUIREMENTS FOR THE DEGREE OF

MASTER OF SCIENCE

IN

THE DEPARTMENT OF CIVIL ENGINEERING

APRIL 2004

Approval of the Graduate School of Natural and Applied Sciences

_____

Prof. Dr. Canan Özgen

Director

I certify that this thesis satisfies all the requirements as a thesis for the degree of Master of Science.

_____

Prof. Dr. Erdal Çokça

Head of the Department

This is to certify that we have read this thesis and that in our opinion it is fully adequate, in scope and quality, as a thesis for the degree of Master of Science.

_____

Assoc. Prof. Dr. İsmail Aydın

Supervisor

Examining Committee Members:

Prof. Dr. Mustafa Göğüş _____

Assoc. Prof. Dr. İsmail Aydın _____

Assoc. Prof. Dr. Ahmet C. Yalçıner _____

Assist. Prof. Dr. Utku Kanoğlu _____

Dr. Şahnaz Tiğrek _____

I hereby declare that all information in this document has been obtained and presented in accordance with academic rules and ethical conduct. I also declare that, as required by these rules and conduct, I have fully cited and referenced all material and results that are not original to this work.

Name, Last name : Özgür Ulaş Kırlangıç

Signature :

ABSTRACT

GENERATION OF SURFACE WAVES DUE TO SUDDEN MOVEMENTS AT THE SEA BOTTOM

Kırlangıç, Özgür Ulaş

M.S., Department of Civil Engineering,
Supervisor: Assoc. Prof. Dr İsmail Aydın
April 2004, 64 Pages

A mathematical model is developed for investigating time dependent surface deformations of a hydrostatic water volume, when it is subjected to a sudden partial collapse or rise of the sea bottom.

The model solves two-dimensional Navier-Stokes Equations on a vertical plane numerically by using *Marker and Cell Method* (*MAC*) for viscous and compressible fluid including all the nonlinear effects in the solution.

For demonstration, a vertical motion was given to a section in a hypothetical reservoir bed within a short time period and the resulting velocity and pressure fields and the surface profile of the water body are obtained. Computational and physical aspects are discussed.

Keywords: Submarine subsidence, surface waves, Marker and Cell (MAC) Method, moving solid boundary, limited compressibility, tsunami.

ÖZ

DENİZ TABANINDA MEYDANA GELEN ANİ HAREKETLER NETİCESİNDE YÜZEY DALGALARI OLUŞUMU

Kırlangıç, Özgür Ulaş

Yüksek Lisans, İnşaat Mühendisliği Bölümü,
Danışman: Doç. Dr İsmail Aydın
Nisan 2004, 64 Sayfa

Deniz tabanında ani bir kısmi çökme veya yükselmeye maruz kalan hidrostatik bir su hacminin zamana bağlı serbest yüzey deformasyonlarını incelemek amacıyla bir matematiksel model oluşturulmuştur.

Viskoz ve sıkıştırılabilir sıvı için Marker and Cell (MAC) Metodu kullanılarak düşey düzlem üzerinde iki-boyutlu Navier-Stokes Denklemlerininin tüm doğrusal olmayan etkilerini içeren sayısal çözümü yapılmıştır.

Gösterim amaçlı olarak, varsayıma dayanan bir rezervuar tabanındaki bir kesite kısa bir zaman aralığı içinde dikey yönde bir hareket verilmiş ve su hacmindeki hız ve basınç alanları ile yüzey profili elde edilmiştir. Çözümün sayısal ve fiziki yönleri tartışılmıştır.

Anahtar kelimeler: Denizaltı çökmeleri, yüzey dalgaları, Marker and Cell (MAC) Metodu, hareketli katı sınır, kısıtlı sıkıştırılabilirlik, tsunami.

Dedicate to My Parents

ACKNOWLEDGEMENTS

I would like to express sincere thanks to Assoc. Prof. Dr. İsmail Aydın for his supervision and guidance throughout the study carried out for this thesis.

I would like to express sincere thanks to my parents for their moral support.

I would like to express sincere thanks to my managers Mr. Galip Sukaya (Earth Tech Inc.), Mr. Andrew Tczap (Earth Tech Inc.), Mr. Mustafa Tanrıverdi (Yapı Merkezi Inc.) and Mrs. Mehnur Özkanoğlu (State Hydraulic Works) for their support and motivation.

TABLE OF CONTENTS

LIST OF FIGURES

FIGURE

LIST OF SYMBOLS

c : Speed of sound

δt : Time increment for the forward time discretization

δx : Width of computational cell, constant

δy_j : Height of computational cell, variable

δyn_j : Vertical distance between the cell centers of the north neighbor cell and the cell in j^{th} row

δys_j : Vertical distance between the cell centers of the south neighbor cell and the cell in j^{th} row

g_x : Body acceleration in x-direction

g_y : Body acceleration in y-direction

γ : Weighting parameter for central differences and donor cell discretization

h : Surface height of fluid

h_i : Surface height at i^{th} discrete column of fluid

h_{max} : Maximum recorded surface height of entire fluid at an instant of time

H : Initial water depth

h_S : Subsidence height

i : Space index in horizontal direction for discrete parameters

j : Space index in vertical direction for discrete parameters

L_R : Reservoir length

L_S : Subsidence length

μ : Absolute viscosity of fluid

n : Time step index for discrete parameters

ν : Kinematic viscosity of fluid

ω : Relaxation parameter for SOR method

p : Pressure per unit mass

P : Pressure

P_{surf} : Pressure on the free surface

ρ : Density

ρ_0 : Mean constant density

σ_{xx} : Normal component of momentum per unit density flowing per unit time in x direction through unit area in x direction

σ_{yy} : Normal component of momentum per unit density flowing per unit time in y direction through unit area in y direction

t : Time

τ_{xy} : Tangential component of momentum per unit density flowing per unit time in y direction through unit area in x direction

τ_{yx} : Tangential component of momentum per unit density flowing per unit time in x direction through unit area in y direction

u : Velocity component in x-direction

v : Velocity component in y-direction

V_S : Subsidence velocity

VF : Fractional volume of fluid

x : Spatial variable in horizontal direction

y : Spatial variable in vertical direction

CHAPTER 1

INTRODUCTION

1.1 General

A two-dimensional mathematical model is developed to simulate the mechanism of generation of surface waves in the sea after a sudden settlement or rise at a certain section of the sea bottom.

Such vertical tectonic ground movement is typical of major earthquakes along the North Anatolian Fault and has been responsible for the generation of tsunami waves in the past (George, 1999).

When the tsunamigenic potential of the Sea of Marmara is assessed, over 40 tsunamis have taken place during the course of an observational period of about 2000 years (Altinok *et al.,* 2001).

The risk of tsunamis in the Marmara coasts and the recent high magnitude earthquakes occurred in the region, motivated this study to develop a powerful tool for prediction of surface waves associated with earthquakes.

1.2 Description of the Problem

The mathematical model being developed aims to solve scenarios similar to the case shown on the hypothetical reservoir in Figure 1.1. All parameters of the problem and the regular geometry of the reservoir can be modified to match any possible real life scenario.

In Figure 1.1, H is the initial water depth, L_R is the reservoir length, L_S is the subsidence length, h_S is the subsidence height and V_S is the subsidence velocity. The third dimension, which is normal to the page, is taken as unity.

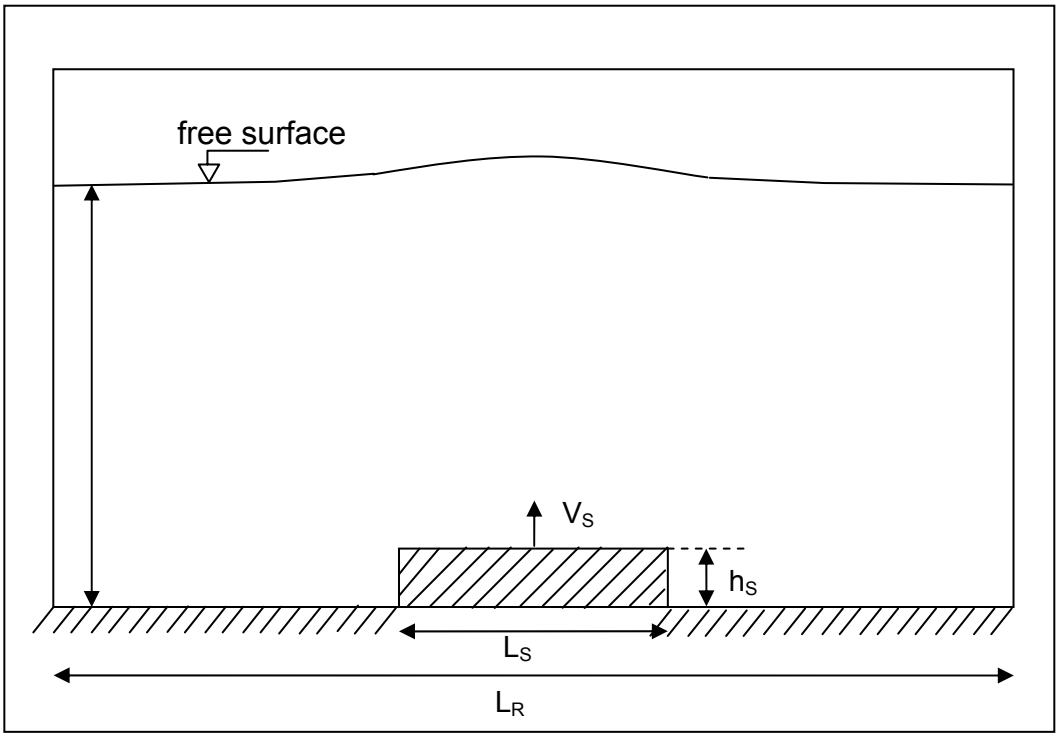

Figure 1.1 – The hypothetical reservoir

At the beginning the flat reservoir bottom is horizontal and hydrostatic water is considered. Then the subsidence volume (boundary) starts to move in vertical direction (upwards or downwards) at a constant velocity. Usually subsidence is completed in a few seconds.

As a result of this vertical ground motion, the hydrostatic water volume in the reservoir gains hydrodynamic acceleration and after short time duration, deformations are observed on the free surface.

Some retardation is expected between the first impulse originated from the sudden ground motion and the first deformation observed on the free surface of the water. This retardation is a result of the compressible property of the fluid. However, the numerical errors accumulated during the transient solution of the system may effect (shortening or extending) this retardation time, but these errors should always stay as a minor factor in an accurate and consistent solution with sufficiently fine mesh and small time increments.

1.3 Literature Survey on Numerical Methods for Solution of the Navier-Stokes Equations

Literature Survey has been carried out in the fields of Computational Fluid Dynamics (CFD), free surface flow modeling methods and fluid compressibility in order to be able to develop a realistic model, which will be capable of solving the scenario described in 1.2.

1.3.1 The Free Surface

A free surface is the interface between a gas and a liquid. Because of the large difference in the densities, the inertia of the gas is generally ignored when compared to the inertia of the liquid. The only influence of the gas on the liquid is then the pressure that it exerts on the liquid surface. Therefore, the liquid is considered to move freely with respect to the gas, and the gas-liquid surface is not constrained, but free.

The presence of a free surface introduces serious complications for any type of analysis. First of all the shape and location of the surface should be described correctly and this information should be available every time when it is needed. Second, this surface shape and location should be evolved with time with a proper algorithm. Third, the free surface boundary conditions must be applied at the surface, at the correct location and at the correct magnitude. (Flow Science Inc.)

1.3.2 The Compressibility

All fluids are compressible and a consequence of the compressibility is that a disturbance introduced at some point will propagate at a finite velocity throughout the medium. The velocity at which the disturbance propagates through the medium is called the Acoustic Velocity or the Speed of Sound. If the medium is assumed to be incompressible then the speed of sound is infinite.

The mathematical modeling of water flow is usually accomplished by assuming that water is incompressible for practical purposes. However this assumption is not valid when the water volume being modeled is relatively large and the distance that a disturbance should travel is relatively long.

1.3.3 Numerical Modeling of Free Surface Flows

There have been many numerical techniques devised for the modeling of free surfaces. Nearly all these techniques can be classified as falling into one of two basic categories, depending on whether they are written primarily in terms of Lagrangian or Eulerian coordinates (Hirt and Cook,1974).

1.3.3.1 Lagrangian Grid

A Lagrangian grid is embedded in the fluid and it moves with the fluid. Since the grid and the fluid move together, free surface is automatically tracked by the grid. This is a simple method of defining and tracking the free surface however it cannot track surfaces that break apart of intersect.

1.3.3.2 Eulerian Grid

An Eulerian grid is fixed and independent from the fluid. Keeping the track of free surface of a fluid moving though an Eulerian grid needs a special scheme working as an auxiliary component of the main solution. However more complicated surface motions can be treated on Eulerian grid.

1.3.3.2.1 Marker and Cell (MAC) Method

The earliest method for the numerical calculation of time dependent viscous incompressible flow with free surface on a fixed Eulerian grid is the Marker and Cell (MAC) Method, which was first introduced by Francis H. Harlow and J. Eddie Welch from University of California, Los Alamos Scientific Laboratory (Harlow and Welch, 1965).

This method uses a set of imaginary marker particles, which are used to indicate the fluid configuration by showing which region is occupied by fluid and which region is empty, such as aluminum dust or hydrogen bubbles are used in an actual laboratory. A cell with no marker particles is marked as an empty cell. A cell with marker particles, lying adjacent to an empty cell, is marked as a surface cell. A cell with marker particles and not in the neighborhood of an empty cell is marked as a full cell. The boundary cells are marked as boundary cells.

The marker particles are initially placed in the cells containing fluid and then they subsequently are moved with local velocity to their next positions at each

time step. A bi-linear interpolation is performed to calculate the velocity with which a particle should move. After moving the particles to their new positions the flagging is done again to represent the new fluid configuration.

MAC Method makes use of finite difference approximations applied to the full Navier-Stokes Equations. The primary dependent variables are the pressure and the two components of velocity. The calculation steps through one cycle of time are as follows:

(1) At the beginning of the cycle, the coordinates of the marker particles and the complete field of cell velocities and cell pressures are known, either as a result of the previous cycle of calculation or from the prescribed initial conditions.

(2) With the completely known field of velocities the corresponding pressure field is calculated for the next time half step to assure that the rate of change of velocity divergence will vanish everywhere until the next time full step. This is done by solving a Poisson equation for pressure field using a suitable relaxation technique.

(3) The new time step velocities are calculated using the known pressure field the two components of accelerations.

(4) The no-slip or free-slip boundary conditions are applied at the rigid walls.

(5) The velocity and the pressure parameters of the free surface boundary cells are calculated by using the free surface boundary conditions.

(6) The marker particles are moved to their next coordinates using the local velocity parameters.

1.3.3.2.2 Improvements to Marker and Cell (MAC) Method

A variety of improvements have contributed to increase in the accuracy and applicability of the original MAC Method, since 1965.

In 1968, Hirt presented a method for investigating the computational stability of finite difference equations, which is applicable to nonlinear equations with variable coefficients. In this paper Hirt also used his method to explain an instability observed in an application of the MAC Method (Hirt, 1968).

In 1968, Hirt and Shannon showed that the free surface boundary conditions that the original MAC Method uses are correct only in the limit of zero viscosity, and they proposed more accurate free surface boundary conditions for viscous flows (Hirt and Shannon, 1968).

In 1969, Daly presented a technique for including the surface tension effects in hydrodynamic calculations, for the fluid flows where the surface tension plays an important role, such as the breakup or coalescence of raindrops or motion of fuel in a space vehicle under low gravity conditions (Daly, 1969).

In 1969, Viecelli proposed a modification to main algorithm of the original MAC in order to be able to treat arbitrary curved solid boundaries (Viecelli, 1969). His method treated to arbitrary curved walls or obstacles as if they were a free surface, to which a pressure is applied such that the particles at the boundary line move tangent it. He showed that a simultaneous iteration on pressures and velocity components is equivalent to the solution of the Poisson equation in the original MAC Method.

In 1970, Chan et al. proposed Stanford University Modified MAC (SUMMAC) Method. In this modified method, they applied the gas pressure just at the interpolated surface locations instead of applying it at the centers of the surface cells, resulting in much more improved accuracy (Chan *et al*., 1970).

In 1971, Nichols and Hirt proposed to apply the correct free surface boundary conditions at the correct location of the free surface (Nichols and Hirt, 1971). In this study they have also showed that the improved MAC with the

complete free surface conditions gives more accurate results than the original MAC, when the results are compared with results of the physical experiments.

In 1971, Viecelli improved his previous work (Viecelli, 1969) of modifying the original MAC. In this latter study he presented Arbitrary Boundary MAC (ABMAC) Method, which is able to treat flows bounded by moving solid walls (Viecelli, 1971).

In 1972, Hirt and Cook developed a computing technique for low-speed fluid dynamics for the calculation of three dimensional flows in the vicinity of one or more block type structures (Hirt and Cook, 1972). The scheme was based on the MAC method but used the simultaneous iteration of pressure and velocities as it was done in (Viecelli, 1969) and (Viecelli, 1971).

In 1973, Nichols and Hirt extended the previous study (Hirt and Cook, 1972). They calculated three-dimensional free surface flows in the vicinity of submerged and exposed structures (Nichols and Hirt, 1973). In this work they used Surface Height Method for keeping the track of the free surface location. They defined the surface height (h) above the bottom of the mesh at the cell center of each vertical column of cells. Then they computed the change in the surface height by solving the following kinematic equation in Cartesian coordinate system,

$$\frac{\partial h}{\partial t} + u\frac{\partial h}{\partial x} = v \qquad (1.1)$$

where u and v are the local surface velocities and t is time.

In 1980, Hirt and Nichols added limited compressibility to the incompressible solutions of hydrodynamic equations for the cases where the compressibility effects are needed for accurate description of the flow (Hirt and Nichols, 1980).

In 1981, Hirt and Nichols illustrated the Volume of Fluid (VOF) Method, which is more flexible and efficient than the other methods for treating complicated free boundary configurations (Hirt and Nichols, 1981). The kinematic equation for the fractional volume of fluid (VF) is given by,

$$\frac{\partial VF}{\partial t} + u\frac{\partial VF}{\partial x} + v\frac{\partial VF}{\partial y} = 0 \qquad (1.2)$$

A unit value of VF corresponds to a cell full of fluid, a zero value of VF corresponds to an empty cell, and a VF value between zero and one contains a free surface.

The original and the improved versions of the MAC Method has been capable of solving a wide range of complicated free-surface flow problems, such as broken dam problem (Harlow and Welch, 1965), impulsive partial opening of a sluice gate (Harlow and Welch, 1965), splash of a liquid drop (Harlow and Shannon, 1967), viscous bore (Hirt and Shannon, 1968), teapot effect (Hirt and Shannon, 1968), fluid falling into the bottom of a circular tank (Viecelli, 1969), flow around a circular cylinder (Viecelli, 1969), motion of a solitary wave in a channel (Chan *et al*., 1970), fluid column rotating about an axis (Nichols and Hirt, 1971), a jet from a nozzle striking a wedge (Viecelli, 1971), jet striking a plate (Viecelli, 1971), flexible bag problem (Viecelli, 1971), and ground motion in generating a water wave (Viecelli, 1971).

1.4 Scope of the Study

The computer program NaSt2D (retrieved from internet, see references) which solves incompressible fluid flows using Marker and Cell (MAC) method was used as the template for the following modifications related to the aims of this study:

i) The numerical infrastructure of the program is revised for a solution on variable mesh in vertical direction.

ii) The effect of limited compressibility (Hirt and Nichols, 1980) is included into the governing equations.

iii) Moving solid boundary is included.

iv) Surface Height Method (Nichols and Hirt, 1973) is added for free surface tracking.

In Chapter II, the discrete Navier-Stokes equations which are used in the model are derived; the boundary conditions applied for the rigid/moving boundaries and the boundary conditions for the free surface boundaries and the method of free surface tracking are discussed. The free surface tracking method that has been used is explained. The stability conditions for the numerical calculations are given and the outline of the solution algorithm is summarized.

In Chapter III, the results of the solution of the hypothetical test cases are presented and discussed.

CHAPTER 2

NUMERICAL SOLUTION OF THE NAVIER-STOKES EQUATIONS

2.1 The Navier-Stokes Equations

The equations of motion describing flow of a compressible fluid are:

$$\frac{\partial \rho}{\partial t} + u\frac{\partial \rho}{\partial x} + v\frac{\partial \rho}{\partial y} + \rho\left(\frac{\partial u}{\partial x} + \frac{\partial v}{\partial y}\right) = 0 \tag{2.1}$$

$$\rho\left(\frac{\partial u}{\partial t} + u\frac{\partial u}{\partial x} + v\frac{\partial u}{\partial y}\right) = \rho g_x - \frac{\partial P}{\partial x} + \mu\left(\frac{\partial^2 u}{\partial x^2} + \frac{\partial^2 u}{\partial y^2}\right) + \frac{\mu}{3}\frac{\partial}{\partial x}\left(\frac{\partial u}{\partial x} + \frac{\partial v}{\partial y}\right) \tag{2.2}$$

$$\rho\left(\frac{\partial v}{\partial t} + u\frac{\partial v}{\partial x} + v\frac{\partial v}{\partial y}\right) = \rho g_y - \frac{\partial P}{\partial y} + \mu\left(\frac{\partial^2 v}{\partial x^2} + \frac{\partial^2 v}{\partial y^2}\right) + \frac{\mu}{3}\frac{\partial}{\partial y}\left(\frac{\partial u}{\partial x} + \frac{\partial v}{\partial y}\right) \tag{2.3}$$

where x and y are the spatial variables in horizontal and vertical directions respectively, t is time, ρ is the density of the fluid, u and v are the velocities in horizontal and vertical directions respectively, P is the pressure, μ is the dynamic viscosity and g_x and g_y are the body accelerations in horizontal and vertical directions respectively.

2.2 Limited Compressibility Model (Hirt and Nichols, 1980)

Fluid pressure is assumed to be only a function of density,

$$\frac{dP}{d\rho} = c^2 \tag{2.4}$$

The parameter c in equation (2.4) is the adiabatic speed of sound. Although c may be time- or space-dependent, it is simply assumed to be constant.

Since the density changes in water will be very small, density is also assumed to be the mean constant density, ρ_0. The mass conservation equation (2.1) can be re-written using equation (2.4) and the constant density assumption,

$$\frac{1}{c^2}\frac{\partial P}{\partial t}+\frac{1}{c^2}\left(u\frac{\partial P}{\partial x}+v\frac{\partial P}{\partial y}\right)+\rho_0\left(\frac{\partial u}{\partial x}+\frac{\partial v}{\partial y}\right)=0 \tag{2.5}$$

Since u/c^2 and v/c^2 will be very small, equation (2.5) can be further simplified and rearranged for pressure in terms of velocity divergence,

$$\frac{\partial P}{\partial t}=-c^2\rho_0\left(\frac{\partial u}{\partial x}+\frac{\partial v}{\partial y}\right) \tag{2.6}$$

Mass conservation equation (2.6) and the momentum equations (2.2) and (2.3) are rearranged for the constant mean density,

$$\frac{\partial u}{\partial x}+\frac{\partial v}{\partial y}=-\frac{1}{c^2}\frac{\partial p}{\partial t} \tag{2.7}$$

$$\frac{\partial u}{\partial t}+u\frac{\partial u}{\partial x}+v\frac{\partial u}{\partial y}=-\frac{\partial p}{\partial x}+g_x+\nu\left(\frac{\partial^2 u}{\partial x^2}+\frac{\partial^2 u}{\partial y^2}\right)+\frac{\nu}{3}\frac{\partial}{\partial x}\left(\frac{\partial u}{\partial x}+\frac{\partial v}{\partial y}\right) \tag{2.8}$$

$$\frac{\partial v}{\partial t}+u\frac{\partial v}{\partial x}+v\frac{\partial v}{\partial y}=-\frac{\partial p}{\partial y}+g_y+\nu\left(\frac{\partial^2 v}{\partial x^2}+\frac{\partial^2 v}{\partial y^2}\right)+\frac{\nu}{3}\frac{\partial}{\partial y}\left(\frac{\partial u}{\partial x}+\frac{\partial v}{\partial y}\right) \tag{2.9}$$

where

$$p=\frac{P}{\rho_0} \tag{2.10}$$

and

$$\nu=\frac{\mu}{\rho_0} \tag{2.11}$$

2.3 Discrete Space Derivative Terms

Staggered grid system is used in which the velocities are defined at the centers of the cell boundaries while pressures are defined at centers of the cells.

The computational mesh is variable in y direction and it gets finer near the lower and upper boundaries while it is coarser in the interior regions. For a cell which on j^{th} row, the cell height is δy_j and the vertical distance of the cell centers of north and south neighbors from the center of the cell are δyn_j and δys_j respectively.

For the ease of use in the numerical procedure, and in computer algorithm, the half step space indices for u and v parameters were replaced with full step space indices in accordance with the staggered grid system.

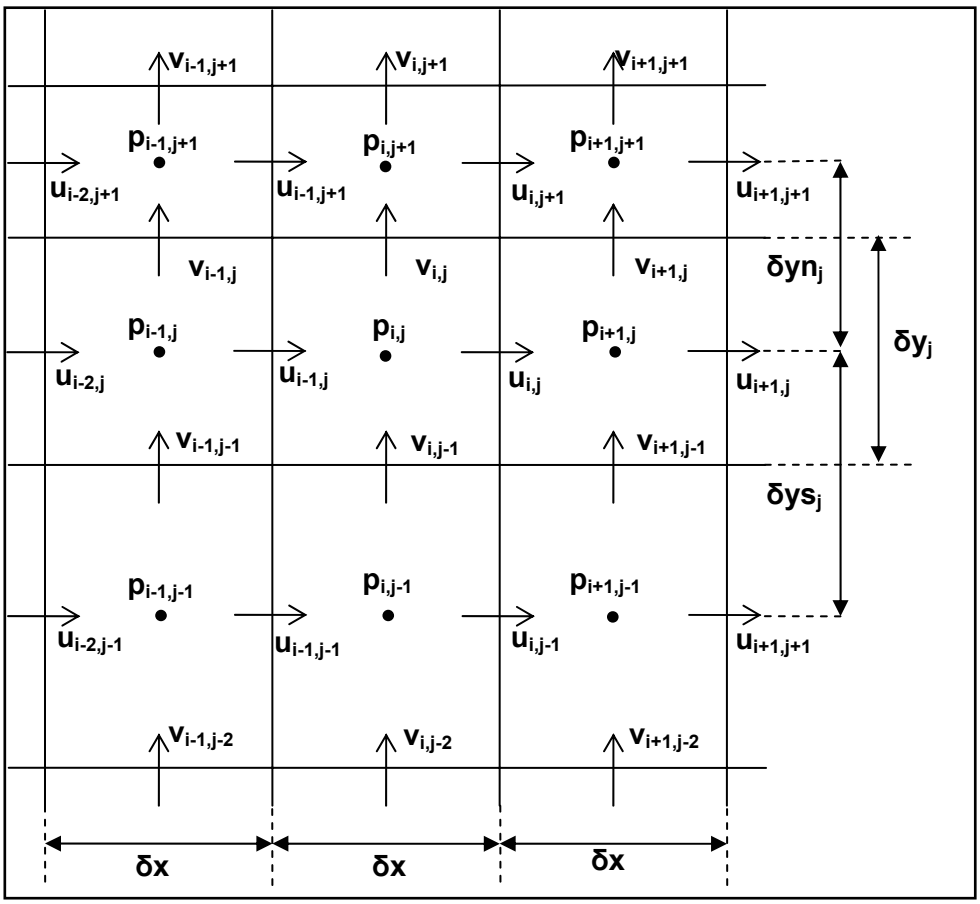

Figure 2.1 – Staggered grid

Since the convective terms in the momentum equations become dominant at high velocities, to avoid stability problems, a mixture of central differences and the donor-cell discretization is used, using the parameter γ in the following formulas which lies between 0.0 and 1.0. For γ =0.0 we recover the central difference discretization, and for γ =1.0, a pure donor-cell scheme results and (Griebel *et al*., 1998).

The space derivative terms of equation (2.8) for the momentum conservation in x-direction are discretized as follows at the mid point of the right edge of the Cell (i,j):

$$\delta ys_j = \frac{\delta y_j + \delta y_{j-1}}{2} \tag{2.12}$$

$$\delta yn_j = \frac{\delta y_{j+1} + \delta y_j}{2} \tag{2.13}$$

$$\left[\frac{\partial u}{\delta x}\right]_{i,j}^{backward} = [DUW]_{i,j} = \frac{u_{i,j} - u_{i-1,j}}{\delta x} \tag{2.14}$$

$$\left[\frac{\partial u}{\delta x}\right]_{i,j}^{forward} = [DUE]_{i,j} = \frac{u_{i+1,j} - u_{i,j}}{\delta x} \tag{2.15}$$

$$\left[\frac{\partial u}{\delta y}\right]_{i,j}^{backward} = [DUS]_{i,j} = \frac{u_{i,j} - u_{i,j-1}}{\delta ys_j} \tag{2.16}$$

$$\left[\frac{\partial u}{\delta y}\right]_{i,j}^{forward} = [DUN]_{i,j} = \frac{u_{i,j+1} - u_{i,j}}{\delta yn_j} \tag{2.17}$$

$$\bar{v}_{i,j} = \frac{v_{i,j} + v_{i+1,j} + v_{i,j-1} + v_{i+1,j-1}}{4} \tag{2.18}$$

$$\delta y_\alpha = \delta yn_j + \delta ys_j + \gamma\, sgn(\bar{v}_{i,j})\left(\delta yn_j - \delta ys_j\right) \tag{2.19}$$

$$\left[u\frac{\partial u}{\delta x}\right]_{i,j} = [UDUDX]_{i,j}$$

$$= \frac{u_{i,j}}{2}\left([DUW]_{i,j} + [DUE]_{i,j} + \gamma\, sgn(u_{i,j})\left([DUW]_{i,j} - [DUE]_{i,j}\right)\right) \quad (2.20)$$

$$\left[v\frac{\partial u}{\partial y}\right]_{i,j} = [VDUDY]_{i,j}$$

$$= \frac{\bar{v}_{i,j}}{\delta y_{\alpha}}\left(\delta yn_j [DUS]_{i,j} + \delta ys_j [DUN]_{i,j}\right)$$

$$+ \frac{\bar{v}_{i,j}}{\delta y_{\alpha}}\gamma sgn(\bar{v}_{i,j})\left(\delta yn_j [DUS]_{i,j} - \delta ys_j [DUN]_{i,j}\right) \quad (2.21)$$

$$\left[\frac{\partial^2 u}{\partial x^2} + \frac{\partial^2 u}{\partial y^2}\right]_{i,j} = [LAPLU]_{i,j}$$

$$= \frac{u_{i+1,j} - 2u_{i,j} + u_{i-1,j}}{(\delta x)^2} \quad (2.22)$$

$$+ \frac{2}{\delta yn_j + \delta ys_j}\left(\frac{u_{i,j+1} - u_{i,j}}{\delta yn_j} - \frac{u_{i,j} - u_{i,j-1}}{\delta ys_j}\right)$$

$$\frac{\partial}{\partial x}\left(\frac{\partial u}{\partial x} + \frac{\partial v}{\partial y}\right) = [COMPX]_{i,j}$$

$$= \frac{u_{i+1,j} - 2u_{i,j} + u_{i-1,j}}{(\delta x)^2} + \frac{v_{i+1,j} - v_{i+1,j-1} - v_{i,j} + v_{i,j-1}}{\delta x \delta y_j} \quad (2.23)$$

$$\left[\frac{\partial p}{\partial x}\right]_{i,j} = \frac{p_{i+1,j} - p_{i,j}}{\delta x} \quad (2.24)$$

The space derivative terms of equation (2.9) for the momentum conservation in y-direction are discretized as follows at the mid point of the upper edge of the Cell (i,j):

$$\delta ys_j = \delta y_j \quad (2.25)$$

$$\delta yn_j = \delta y_{j+1} \quad (2.26)$$

$$\left[\frac{\partial v}{\delta x}\right]_{i,j}^{backward} = [DVW]_{i,j} = \frac{v_{i,j} - v_{i-1,j}}{\delta x} \tag{2.27}$$

$$\left[\frac{\partial v}{\delta x}\right]_{i,j}^{forward} = [DVE]_{i,j} = \frac{v_{i+1,j} - v_{i,j}}{\delta x} \tag{2.28}$$

$$\left[\frac{\partial v}{\delta y}\right]_{i,j}^{backward} = [DVS]_{i,j} = \frac{v_{i,j} - v_{i,j-1}}{\delta ys_j} \tag{2.29}$$

$$\left[\frac{\partial v}{\delta y}\right]_{i,j}^{forward} = [DVN]_{i,j} = \frac{v_{i,j+1} - v_{i,j}}{\delta yn_j} \tag{2.30}$$

$$\bar{u}_{i,j} = \frac{\delta ys_j(u_{i,j+1} + u_{i-1,j+1}) + \delta yn_j(u_{i,j} + u_{i-1,j})}{2(\delta ys_j + \delta yn_j)} \tag{2.31}$$

$$\delta y_\alpha = \delta yn_j + \delta ys_j + \gamma\, sgn(v_{i,j})\left(\delta yn_j - \delta ys_j\right) \tag{2.32}$$

$$\left[u\frac{\partial v}{\delta x}\right]_{i,j} = [UDVDX]_{i,j}$$
$$= \frac{\bar{u}_{i,j}}{2}\left([DVW]_{i,j} + [DVE]_{i,j} + \gamma\, sgn(\bar{u}_{i,j})\left([DVW]_{i,j} - [DVE]_{i,j}\right)\right) \tag{2.33}$$

$$\left[v\frac{\partial v}{\partial y}\right]_{i,j} = [VDVDY]_{i,j}$$
$$= \frac{v_{i,j}}{\delta y_\alpha}\left(\delta yn_j[DVS]_{i,j} + \delta ys_j[DVN]_{i,j}\right)$$
$$+ \frac{v_{i,j}}{\delta y_\alpha}\gamma sgn(v_{i,j})\left(\delta yn_j[DVS]_{i,j} - \delta ys_j[DVN]_{i,j}\right) \tag{2.34}$$

$$\left[\frac{\partial^2 v}{\partial x^2}+\frac{\partial^2 v}{\partial y^2}\right]_{i,j}=[\mathrm{LAPLV}]_{i,j}$$
$$=\frac{v_{i+1,j}-2v_{i,j}+v_{i-1,j}}{(\delta x)^2}$$
$$+\frac{2}{\delta ys_j+\delta yn_j}\left(\frac{v_{i,j+1}-v_{i,j}}{\delta yn_j}-\frac{v_{i,j}-v_{i,j-1}}{\delta ys_j}\right) \quad (2.35)$$

$$\frac{\partial}{\partial y}\left(\frac{\partial u}{\partial x}+\frac{\partial v}{\partial y}\right)=[\mathrm{COMPY}]_{i,j}$$
$$=\frac{2\left(u_{i,j+1}-u_{i,j}-u_{i-1,j+1}+u_{i-1,j}\right)}{\delta x(\delta ys_j+\delta yn_j)}$$
$$+\frac{2}{\delta ys_j+\delta yn_j}\left(\frac{v_{i,j+1}-v_{i,j}}{\delta yn_j}-\frac{v_{i,j}-v_{i,j-1}}{\delta ys_j}\right) \quad (2.36)$$

$$\left[\frac{\partial p}{\partial y}\right]_{i,j}=\frac{2\left(p_{i,j+1}-p_{i,j}\right)}{(\delta y_{j+1}+\delta y_j)} \quad (2.37)$$

2.4 Forward Time Discretization

The time discretization for the equations (2.8) and (2.9) are written in forward full time steps for velocity parameters. For simplicity, the velocity parameters at the n^{th} time level are shown without index.

The pressure parameters within the forward time discretizations of equations (2.8) and (2.9) are at $(n+1/2)^{th}$ time level relative to velocity parameters. However, for simplicity no time level index is used for the pressure parameters which are at the $(n+1/2)^{th}$ time level; and p parameters which are at $(n-1/2)^{th}$ time level are shown as $p^{(old)}$.

The velocity components are updated using the momentum equations,

$$u_{i,j}^{n+1}=u_{i,j}+\delta t\left(g_x+\nu[\mathrm{LAPLU}]_{i,j}+\frac{1}{3}\nu[\mathrm{COMPX}]_{i,j}\right)$$
$$-\delta t\left([\mathrm{UDUDX}]_{i,j}+[\mathrm{VDUDY}]_{i,j}+\frac{p_{i+1,j}-p_{i,j}}{\delta x}\right) \quad (2.38)$$

$$v_{i,j}^{n+1} = v_{i,j} + \delta t\left(g_y + \nu[\mathrm{LAPLV}]_{i,j} + \frac{1}{3}\nu[\mathrm{COMPY}]_{i,j} \right) - \delta t\left([\mathrm{UDVDX}]_{i,j} + [\mathrm{VDVDY}]_{i,j} + \frac{2(p_{i,j+1} - p_{i,j})}{(\delta y_{j+1} + \delta y_j)} \right) \quad (2.39)$$

By defining F and G functions, all the terms, which are at n^{th} time step, can be made more compact for the later uses in equations,

$$F_{i,j} = u_{i,j} + \delta t\left(g_x + \nu[\mathrm{LAPLU}]_{i,j} + \frac{1}{3}\nu[\mathrm{COMPX}]_{i,j} \right) - \delta t\left([\mathrm{UDUDX}]_{i,j} + [\mathrm{VDUDY}]_{i,j} \right) \quad (2.40)$$

$$G_{i,j} = v_{i,j} + \delta t\left(g_y + \nu[\mathrm{LAPLV}]_{i,j} + \frac{1}{3}\nu[\mathrm{COMPY}]_{i,j} \right) - \delta t\left([\mathrm{UDVDX}]_{i,j} + [\mathrm{VDVDY}]_{i,j} \right) \quad (2.41)$$

Equations (2.38) and (2.39) can be re-written in a more simple way, in terms of F and G functions,

$$u_{i,j}^{n+1} = F_{i,j} - \delta t\left(\frac{p_{i+1,j} - p_{i,j}}{\delta x} \right) \quad (2.42)$$

$$v_{i,j}^{n+1} = G_{i,j} - \delta t \frac{2(p_{i,j+1} - p_{i,j})}{(\delta y_{j+1} + \delta y_j)} \quad (2.43)$$

Pressure terms of the next half time step, which are required in equations (2.42) and (2.43), in order to be able to calculate the next time step velocities will be determined from the condition of mass conservation, which is given in equation (2.7).

The mass conservation equation (2.7) is written in discrete form at the mid point of Cell (i,j) using the next time step velocities. Satisfaction of this equation guarantees the conservation of mass at the next time step.

$$\left[\frac{\partial u}{\partial x}+\frac{\partial v}{\partial y}\right]_{i,j}=\frac{F_{i,j}-F_{i-1,j}}{\delta x}+\frac{G_{i,j}-G_{i,j-1}}{\delta y_j}-\delta t\left(\frac{p_{i+1,j}-2p_{i,j}+p_{i-1,j}}{\delta x^2}\right)$$
$$-\frac{2\delta t}{\delta y_j}\left(\frac{p_{i,j+1}-p_{i,j}}{\delta y_{j+1}+\delta y_j}-\frac{p_{i,j}-p_{i,j-1}}{\delta y_j+\delta y_{j-1}}\right) \quad (2.44)$$

$$\left[\frac{\partial p}{\partial t}\right]_{i,j}=\frac{p_{i,j}}{\delta t}-\frac{p_{i,j}^{(old)}}{\delta t} \quad (2.45)$$

Equation (2.7) is written again with the terms discretized in equations (2.44) and (2.45);

$$-\frac{1}{c^2}\left(\frac{p_{i,j}}{\delta t}-\frac{p_{i,j}^{(old)}}{\delta t}\right)=\frac{F_{i,j}-F_{i-1,j}}{\delta x}+\frac{G_{i,j}-G_{i,j-1}}{\delta y_j}-\delta t\left(\frac{p_{i+1,j}-2p_{i,j}+p_{i-1,j}}{\delta x^2}\right)$$
$$-\frac{2\delta t}{\delta y_j}\left(\frac{p_{i,j+1}-p_{i,j}}{\delta y_{j+1}+\delta y_j}-\frac{p_{i,j}-p_{i,j-1}}{\delta y_j+\delta y_{j-1}}\right) \quad (2.46)$$

Equation (2.46) is rearranged to leave the terms at (n+1/2) time level at the left side of the equation,

$$\frac{1}{c^2}\frac{p_{i,j}}{\delta t^2}-\left(\frac{p_{i+1,j}-2p_{i,j}+p_{i-1,j}}{\delta x^2}\right)-\frac{2}{\delta y_j}\left(\frac{p_{i,j+1}-p_{i,j}}{\delta y_{j+1}+\delta y_j}-\frac{p_{i,j}-p_{i,j-1}}{\delta y_j+\delta y_{j-1}}\right)$$
$$=\frac{1}{c^2}\frac{p_{i,j}^{(old)}}{\delta t^2}-\frac{1}{\delta t}\left(\frac{F_{i,j}-F_{i-1,j}}{\delta x}+\frac{G_{i,j}-G_{i,j-1}}{\delta y_j}\right) \quad (2.47)$$

$$[RHS]_{i,j}=\frac{1}{\delta t}\left(\frac{F_{i,j}-F_{i-1,j}}{\delta x}+\frac{G_{i,j}-G_{i,j-1}}{\delta y_j}\right)-\frac{1}{c^2}\frac{p_{i,j}^{(old)}}{\delta t^2} \quad (2.48)$$

Equation (2.47) is rearranged for $p_{i,j}$ at the left side of the equation,

$$\left(\frac{1}{c^2\delta t^2}+\frac{2}{\delta x^2}+\frac{2(\delta y_{j+1}+2\delta y_j+y_{j-1})}{\delta y_j(\delta y_{j+1}+\delta y_j)(\delta y_j+\delta y_{j-1})}\right)p_{i,j}$$
$$=\frac{p_{i+1,j}+p_{i-1,j}}{\delta x^2}+\frac{2}{\delta y_j}\left(\frac{p_{i,j+1}}{(\delta y_{j+1}+\delta y_j)}+\frac{p_{i,j-1}}{(\delta y_j+\delta y_{j-1})}\right)-[RHS]_{i,j} \quad (2.49)$$

Equation (2.49) is rearranged for the iterative solution of $p_{i,j}$ with Successive Over Relaxation (SOR) method, where ω is the relaxation parameter in the interval [0,2],

$$\text{beta}\_2 = -\frac{\varpi}{\left(\frac{1}{c^2\delta t^2}+\frac{2}{\delta x^2}+\frac{2(\delta y_{j+1}+2\delta y_j+y_{j-1})}{\delta y_j(\delta y_{j+1}+\delta y_j)(\delta y_j+\delta y_{j-1})}\right)} \tag{2.50}$$

$$p_{i,j}^{iter+1} = (1-\varpi)p_{i,j}^{iter} + \text{beta}\_2*\left[\text{RHS}\right]_{i,j} - \text{beta}\_2*\left(\frac{p_{i+1,j}^{iter}+p_{i-1,j}^{iter+1}}{\delta x^2}+\frac{2}{\delta y_j}\left(\frac{p_{i,j+1}^{iter}}{\delta y_{j+1}+\delta y_j}+\frac{p_{i,j-1}^{iter+1}}{\delta y_j+\delta y_{j-1}}\right)\right) \tag{2.51}$$

$$\text{res} = \frac{p_{i+1,j}-2p_{i,j}+p_{i-1,j}}{\delta x^2}+\frac{2}{\delta y_j}\left(\frac{p_{i,j+1}-p_{i,j}}{\delta y_{j+1}+\delta y_j}-\frac{p_{i,j}-p_{i,j-1}}{\delta y_j+\delta y_{j-1}}\right) - [\text{RHS}]_{i,j} - \frac{1}{c^2}\frac{p_{i,j}}{\delta t^2} \tag{2.52}$$

2.5 The Boundary Conditions for the Rigid/Moving Solid Boundaries

In the original Marker and Cell Method the solid boundaries are considered to be fixed, in other words not in motion. This is done by taking the normal velocity on the solid boundary face as zero, and deriving the fictitious velocity and pressure values inside the boundary cell accordingly.

However, in this study a part of the solid boundary is in motion in the reservoir bed and the normal velocity on the solid boundary face is not always zero. So, the fictitious velocity and pressure parameters for the application of solid boundary condition should be derived keeping the normal velocity on the solid face in the equations.

In addition, depending on the computational model, a solid boundary can be assumed to be either of two types, no-slip or free-slip, and the fictitious tangential velocities are determined according to the type of the boundary.

The mass and momentum conservation equations, which are written for the fluid cells in the neighborhood of the solid boundaries, refer to the fictitious pressure and the tangential velocities within the solid boundary cells.

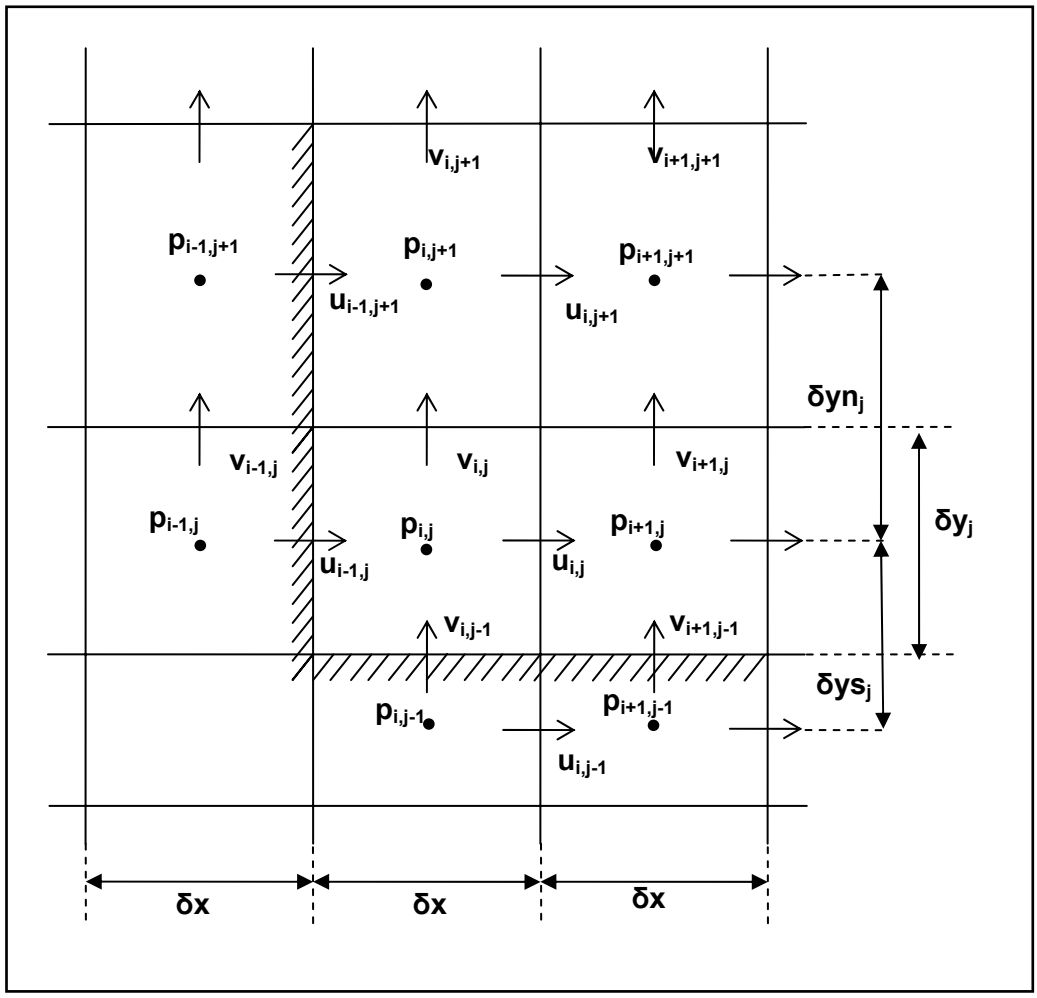

Figure 2.2 – Solid boundary

The fictitious velocities should be consistent with the boundary type. For the sample solid boundary given in Figure 2.2, the fictitious velocities are derived for both free slip and no slip cases;

Free-slip solid boundary:

$$v_{i-1,j} = v_{i,j} \tag{2.53}$$

$$u_{i,j-1} = u_{i,j} \tag{2.54}$$

No-slip solid boundary:

$$v_{i-1,j} = -v_{i,j} \tag{2.55}$$

$$u_{i,j-1} = -u_{i,j} \tag{2.56}$$

The fictitious pressure in a solid boundary is referred during the solution of the Poisson equation for the pressure of the internal fluid cells. In fact, the Poisson equation is derived from the condition of conservation of mass in a cell.

The discrete form of the conservation of mass condition was given in equation (2.46). In equation (2.46) the unknown velocities of next time step are written in terms of known F and G functions of previous time and pressures of the next half time step as given in equations (2.42) and (2.43).

When the Cell (i,j) in Figure (2.2) is considered the velocities $u_{i-1,j}$ and $v_{i,j-1}$ are equal to the normal velocity of the solid wall. In either case the normal velocities on the solid walls are always known.

Since the left sides of the equations (2.42) and/or (2.43) are always known for the fluid cells in the neighborhood of solid boundaries, the parameters on the right side of the equations (2.42) and/or equation (2.43) can be chosen arbitrarily. The simplest choice is setting the fictitious pressure equal to the pressure of the neighboring fluid and setting the F and G functions that are on the wall faces equal to the normal velocity of the wall.

$$F_{i-1,j} = u_{i,j} \tag{2.57}$$

$$G_{i,j-1} = v_{i,j-1} \tag{2.58}$$

Thus,

$$p_{i-1,j} = p_{i,j} \tag{2.59}$$

$$p_{i,j-1} = p_{i,j} \tag{2.60}$$

2.6 Boundary Conditions for the Free Surface

The only influence of the gas on the liquid on a free surface is assumed to be the normal pressure it exerts on the fluid. The correct free-surface boundary conditions are the conservation of mass in the surface cells and vanishing of the normal and tangential stresses.

In the scope of this study, the surface tension effects (assuming low curvature at the surface) and the compressibility in free surface cells (since the change in the pressure with respect to time will be very small in a surface cell) are ignored during the derivation of boundary conditions for the free surface cells.

Mass conservation condition in a free surface cell is satisfied with the incompressible continuity equation,

$$\frac{\partial u}{\partial x} + \frac{\partial v}{\partial y} = 0 \tag{2.61}$$

According to Stokes' viscosity law for a Newtonian fluid the stresses are linearly related to rates of deformation. The stress-rate of deformation relations for an incompressible fluid are given in the following equations,

$$\sigma_{xx} = -p + 2\nu\frac{\partial u}{\partial x} \tag{2.62}$$

$$\sigma_{yy} = -p + 2\nu\frac{\partial v}{\partial y} \tag{2.63}$$

$$\tau_{xy} = \tau_{yx} = \nu\left(\frac{\partial u}{\partial y} + \frac{\partial v}{\partial x}\right) \tag{2.64}$$

Since wave height is relatively small compared to the length of the wave we can assume a nearly horizontal free surface while deriving the free surface

boundary conditions. Using this assumption we can take the normal stress as σ_{yy} and tangential stress as τ_{yx} on the free surface cell.

Since there is no flux of momentum through the free surface, the boundary condition is

$$\sigma_{yy} = -p + 2\nu\frac{\partial v}{\partial y} = 0 \tag{2.65}$$

$$\tau_{yx} = \nu\left(\frac{\partial u}{\partial y} + \frac{\partial v}{\partial x}\right) = 0 \tag{2.66}$$

These equations are rearranged and the normal and tangential stress conditions at the free surface are obtained,

(1) normal stress condition:

$$p = 2\nu\frac{\partial v}{\partial y} \tag{2.67}$$

(2) tangential stress condition:

$$\frac{\partial u}{\partial y} + \frac{\partial v}{\partial x} = 0 \tag{2.68}$$

The normal velocity on the surface is computed from the condition of conservation of mass given in equation 2.61,

$$v_{i,j} = v_{i,j-1} - \delta y_j\left(\frac{u_{i,j} - u_{i-1,j}}{\delta x}\right) \tag{2.69}$$

The tangential velocity $u_{i-1,j+1}$ is computed from the tangential stress condition given in equation 2.68,

$$u_{i-1,j+1} = u_{i-1,j} - \frac{\delta yn_j}{\delta x}(v_{i,j} - v_{i-1,j}) \tag{2.70}$$

The pressure on the free surface is computed from the normal stress condition given in equation 2.67.

$$p_{surf} = 2\nu\left(\frac{v_{i,j} - v_{i,j-1}}{\delta y_j}\right) \tag{2.71}$$

The pressure to be assigned to the center of the surface cell is calculated by a linear interpolation using the interpolation factor η. The interpolation factor η is the ratio of grid space between the cell centers (δys_j) to the distance from the actual surface to the center of neighboring full cell (d),

$$\eta = \delta ys_j / d \tag{2.72}$$

$$p_{i,j} = \eta p_{surf} + (1-\eta) p_{i,j-1} \tag{2.73}$$

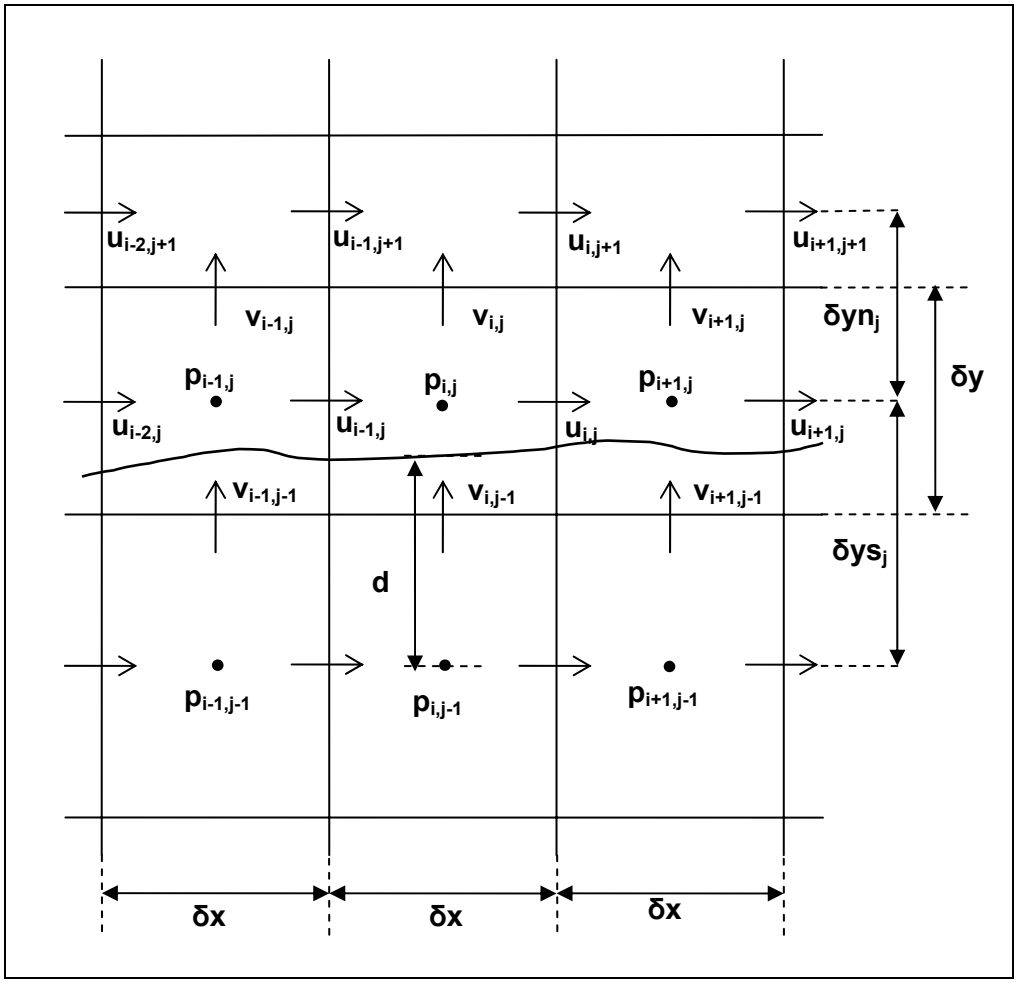

Figure 2.3 – The free surface

2.7 The Surface Height Method

Location of the fluid surface is tracked by the height of fluid (h_i) with respect to the bottom of the mesh for each vertical column of cells. The cell in which the height of fluid h_i stays within the upper and lower cell borders is flagged as a surface cell and all the remaining cells below this surface cell are flagged as full cells.

The change in the surface profile is determined by the local fluid velocity, i.e. the vertical component of the fluid motion plus the horizontal convection of the surface elevation from adjacent cell columns,

$$\frac{\partial h}{\partial t} = v - u\frac{\partial h}{\partial x} \tag{2.74}$$

Equation 2.74 is written in finite difference form using a space centered and forward in time method by adding a positive diffusion term in order to compensate the negative diffusion truncation error as explained (Nichols and Hirt, 1973).

$$h_{i,j}^{n+1} = h_{i,j}^{n} + \delta t\left(\overline{v}_{i,j}^{n+1} + \frac{(u_{i,j}^{n+1} + u_{i-1,j}^{n+1})(h_{i-1,j}^{n} - h_{i+1,j}^{n})}{4\delta x}\right) + \gamma\left(\frac{h_{i+1,j}^{n} - 2h_{i,j}^{n} + h_{i-1,j}^{n}}{\delta x^{2}}\right) \tag{2.75}$$

The vertical velocity of the fluid motion, $\overline{v}_{i,j}^{n+1}$,is the velocity at the surface, and it is obtained by a linear interpolation within the cell.

2.8 The Stability Conditions for the Numerical Calculations

The numerical calculations sometimes can give large, high frequency oscillations in space, time or both. This behavior is referred to as numerical instability. If the calculated results show significant variations over distances comparable to a cell width or over times comparable to a time increment, the accuracy of the solutions cannot be relied on.

To prevent this type of numerical instability and inaccuracy, there are restrictions in determining the dimensions of the computational cells δx and δy, the time increment δt, and the weighting parameter γ.

For accuracy, the dimensions of the computational cells δx and δy should be selected small enough to resolve the expected spatial variations in all dependent variables.

After selecting the mesh dimensions to obtain an acceptable resolution, then the time increment should be chosen which has got two restrictions.

First, since the finite difference equations assume fluxes only between adjacent cells, the fluid cannot move through more than one cell in one time step. This restriction is given as,

$$\delta t < \min\left\{ \frac{\delta x}{|u_{i,j}|}, \frac{\delta y_j}{|v_{i,j}|} \right\} \tag{2.76}$$

Hirt suggests using one fourth to one third of the minimum time increment found in equation 2.76 (Hirt and Nichols, 1981).

Second, for the viscous flows, i.e. the kinematic viscosity is nonzero; the momentum must not diffuse more than approximately one cell in one time step. This restriction is given as,

$$\nu\delta t < \frac{1}{2}\left(\frac{1}{\delta x^2} + \frac{1}{\delta y_j^{\,2}} \right)^{-1} \tag{2.77}$$

The minimum of the time increments found in the equations 2.76 and 2.77 is selected for every adaptive time step.

After selecting the space and time increments the weighting parameter γ is chosen from,

$$1 \geq \gamma > \max\left\{ \frac{|u_{i,j}|\delta t}{\delta x}, \frac{|v_{i,j}|\delta t}{\delta y_j} \right\} \tag{2.78}$$

Hirt suggests 1.2 to 1.5 times the right hand member of equation 2.78 for the good choice of γ (Hirt and Nichols, 1981). It is also mentioned that a too large γ may introduce an unnecessary amount of numerical smoothing (diffusion like truncation errors).

2.9 Outline of the Solution Algorithm

1) All the case dependent parameters used in the solution are read from the input data file.

2) The variable mesh is read from the mesh data file.

3) The topography of the reservoir bed is read from profile data file.

4) Each cell is flagged as FULL, EMPTY or SURFACE according to the initial free surface level of the reservoir.

5) The initial values of the velocity and pressure parameters are assigned to each computational cell.

6) The fictitious velocity and pressure parameters inside the solid boundaries are calculated.

7) The time loop starts:

   1. The new instantaneous velocity of the moving section of the ground is assigned to the moving boundary cells.

   2. The allowable time step is determined from the stability conditions of the numerical method (equations 2.76 and 2.77).

   3. The computational cells are flagged as FULL, EMPTY or SURFACE according to the location of free surface which is represented by a h_i value for each column of cells.

   4. The free surface boundary conditions are applied to the free surface cells.

   5. The F and G functions are calculated for each fluid cell including surface cells.

   6. The RHS function is calculated for each FULL fluid cell.

   7. The pressures at the center of FULL cells are calculated iteratively using Successive Over Relaxation (SOR) Method. At

the beginning of every iteration cycle, the pressure values of the free surface and the wall boundary cells are updated.

8. The new velocity field is calculated.

9. The moving boundary is moved to its next location using the instantaneous wall velocity.

10. The fictitious velocity and pressure parameters inside the solid boundaries are calculated.

11. The free surface boundary conditions are applied to the free surface cells.

12. The free surface is advanced to its new position by solving the height of fluid function.

13. The computed parameters u, v, p, h, volume and h_{max} are written to the output files.

14. The time loop ends.

CHAPTER 3

RESULTS AND DISCUSSIONS

3.1 Results

For demonstration of the mathematical model, two hypothetical reservoirs of different dimensions are selected. Then the scenario described in Chapter 1.2 is applied to both cases.

General sketch of the flow domain was given in Figure 1.1. The reservoir bottom is defined as a no-slip boundary and the vertical side walls are defined as free-slip boundaries.

The mass density of water is 1000 kg/m^3, kinematic viscosity of water is 10^{-6} m^2/s and speed of sound in water is 1482 m/s. The gravitational acceleration is 9.81 m/s^2.

The initial decision on the mesh sizes to be used has been made by keeping the following physical aspects in mind.

The free surface is relatively free in motion and its orientation is very sensitive to the small variations in the field variables. On the other hand, the free surface is the boundary of the fluid domain where all the internal computations are performed. So the outputs of the internal computations are strongly affected by the orientation of the free surface and the boundary conditions applied on it. Any error made in representing the correct orientation of the free surface and applying the correct free surface boundary conditions results in accumulation of errors, which are also amplified because of the mutual interaction of the free surface and the internal fluid domain. As a result, the vertical mesh near the free surface should be fine enough to be able to minimize these errors.

On the other hand, the shock wave created by the vertical and rapid motion of the ground is the source of energy that initiates the hydrodynamic motion, which is the main subject of this study. This shock wave should be captured as accurate as possible for consistent solutions. As a result, the vertical mesh near the reservoir bed should be fine enough.

The model needs a finer mesh near the zones where there is rapid variations in the hydrodynamic parameters. However, because of the compressible character of the fluid after the sudden excitation, a vibrating motion is observed throughout the entire volume. Because of this vibration the parameters of the interior regions of the water volume also show variations with respect to time and space. There is an advantage of grid refining near the boundaries however selection of excessively coarse mesh sizes in the interior regions is not possible.

The final decision on the mesh sizes to be used has been made by testing the calculations on different mesh alternatives checking out if the instantaneous volumes are conserved and if the outputs of alternative mesh sizes are consistent. This grid refinement test is carried out both in horizontal and vertical directions for each of the problem case. At the end of the test the optimum horizontal mesh size δx and the optimum vertical mesh sizes δy_{min} and δy_{max} are determined.

3.1.1 Hypothetical Case I (0.1 km Depth)

The hypothetical reservoir is 1 km long (L_R) and the initial steady state hydrostatic water depth (H) is 0.1 km. At t=1 sec, subsidence volume (L_S=0.1 km) in the middle of the reservoir bed starts to move upwards in vertical direction with a constant velocity of 1 m/s. The motion continues until t=3 sec and this partial section of the reservoir bed rises 2 m in elevation.

Determination of optimum horizontal mesh:

For the determination of optimum horizontal mesh, three different δx alternatives are tested on the same problem keeping every other parameter constant. The outputs of the computations are then compared and a decision is made.

The fluid volume in the computational domain is computed and recorded at every time step. The instantaneous volumes are then divided by the initial volume, which normalizes the asymptotical value to unity.

The instantaneous volume/initial volume graphs for δx=2m, δx=5m and δx=10m alternatives on a vertical mesh (δy_{min}=0.25 m, δy_{max}=1.66 m and j_{max}=125) are given in Figure 3.1.

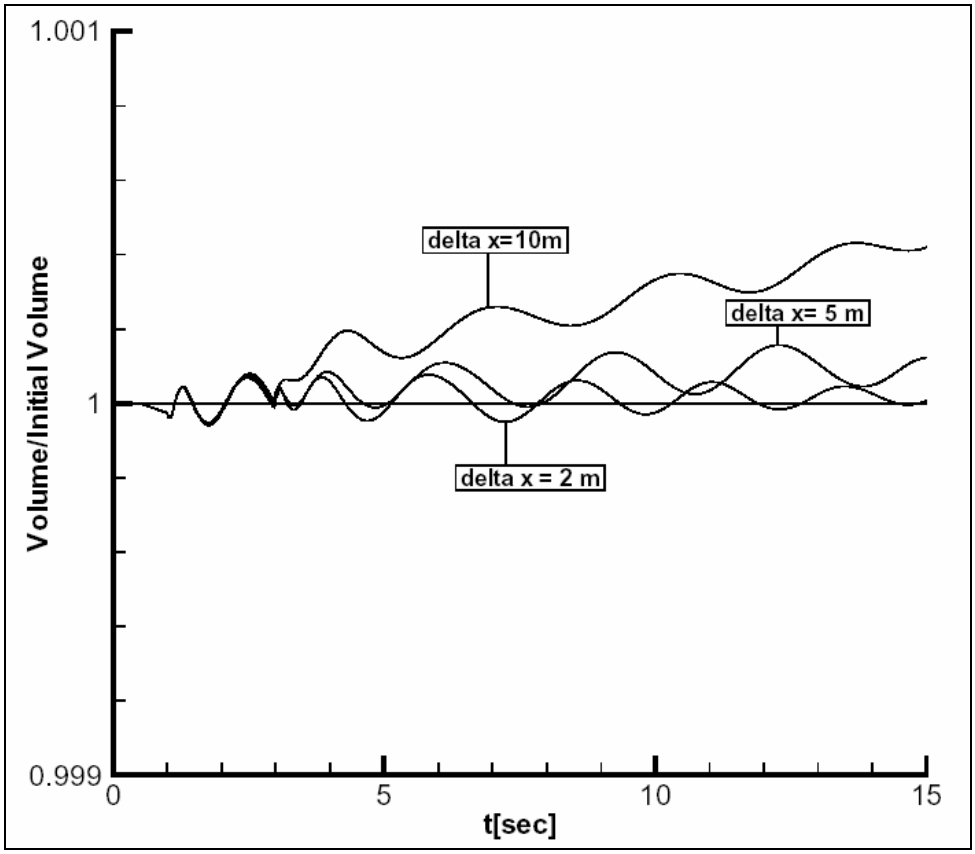

Figure 3.1 – Instantaneous volume/initial volume for Case I (using vertical mesh parameters of δy_{min}=0.25 m, δy_{max}=1.66 m and jmax=125)

From Figure 3.1 it is interpreted that on a coarse horizontal mesh size of δx=10m, the volume of the water has an increasing tendency, which is unphysical and unacceptable. However, for the finer meshes of δx=5m and

δx=2m the volume changes are small and does not show an accumulating behavior and the divergence from unity is tolerable.

Although the mass conservation seems to be satisfied, the consistency of the results should also be checked. Figure 3.2 shows the maximum-recorded water height in the entire reservoir. The consistency of the solutions can be checked using this parameter.

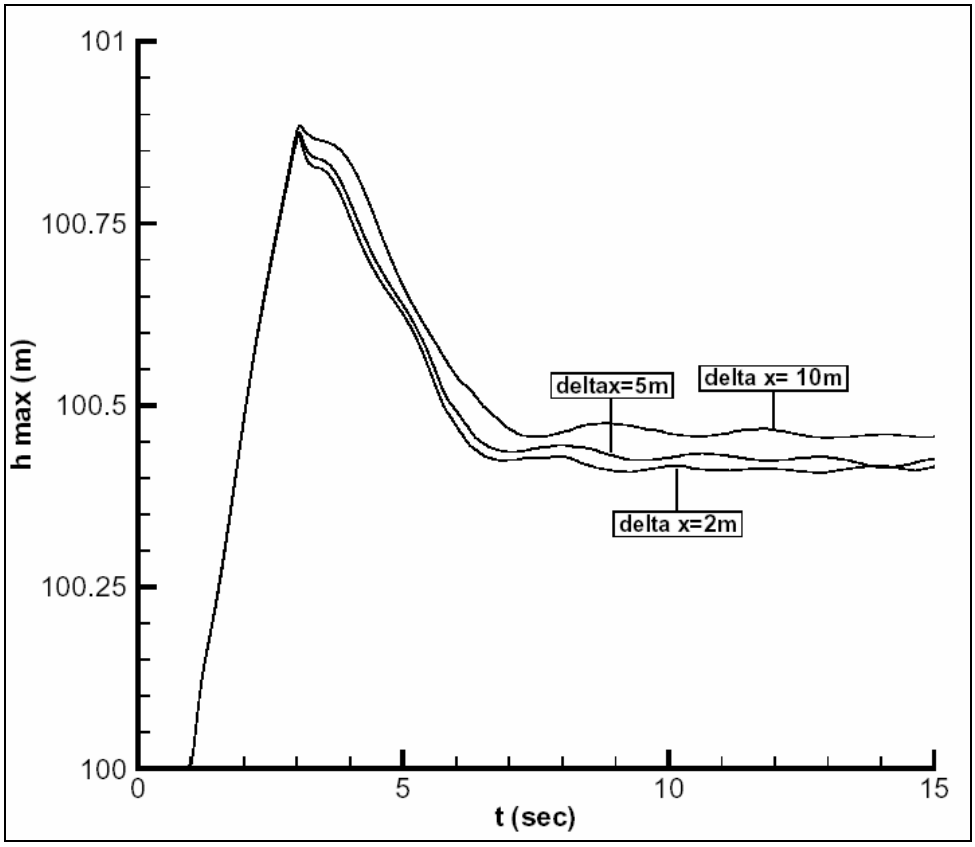

Figure 3.2 – Maximum water level on horizontal mesh alternatives for Case I (using vertical variable mesh of δy_{min}=0.25 m, δy_{max}=1.66 m and jmax=125)

From Figure 3.2 it is interpreted that as the horizontal mesh δx is refined the solution converges to a certain value. The graphs for δx=2m, δx=5m and δx=10m are all consistent in shape and small differences in values are tolerable.

Determination of optimum vertical mesh:

It is known a priori that the field variables change more rapidly in vertical direction than in horizontal direction. Because of this much smaller vertical spacing than horizontal spacing is used especially near the free surface and reservoir bottom.

The sufficiency of the vertical mesh used in the above tests is tested by solving the same problem using a two times finer vertical mesh. In the test the constant horizontal mesh size is taken as δx=2m.

The maximum-recorded water levels graph for the two vertical meshes is given in Figure 3.3.

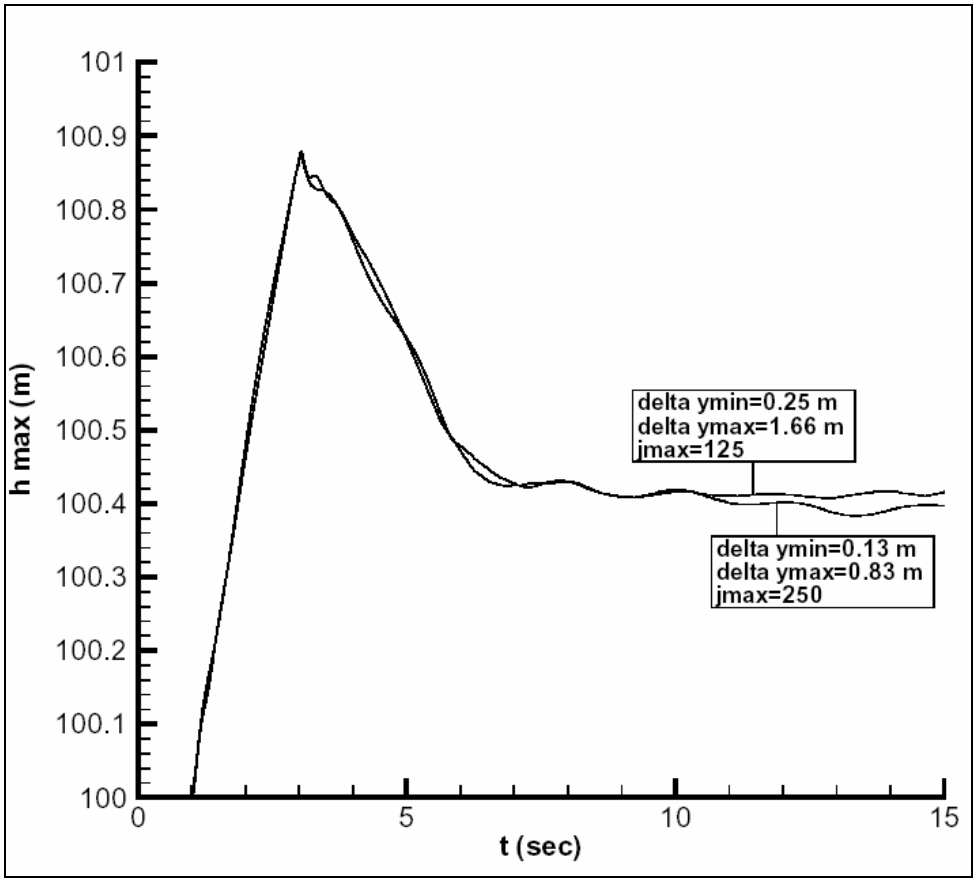

Figure 3.3 – Maximum water level on vertical mesh alternatives on δx=2m for Case I

The graphs given in Figure 3.3 prove the consistency of the results of two different vertical mesh alternatives.

Finally, for the solution of Hypothetical Case I the computational mesh is set uniform in horizontal direction having a constant width (δx=2m). In vertical direction, the mesh is set variable which gets finer near the free surface and at the reservoir bottom (δy_{min}=0.13m), and gets coarser in the interior regions (δy_{max}=0.83 m).

As a result the total computational area, which covers an area of 1000 m x 105 m including the empty cells, is divided into 500 x 250 rectangular cells.

Verification of Reservoir Length and Side Boundary Conditions:

When the main concern is to investigate the initial surface wave which is created under open sea conditions then the reservoir length L_R should be sufficiently large in order to minimize the effect of vertical side boundary conditions which are at the right and left boundaries of the computational domain.

To check whether L_R = 1 km is sufficient, the same problem is solved for three L_R alternatives (Figure 3.4) and convergence at L_R = 1 km is verified.

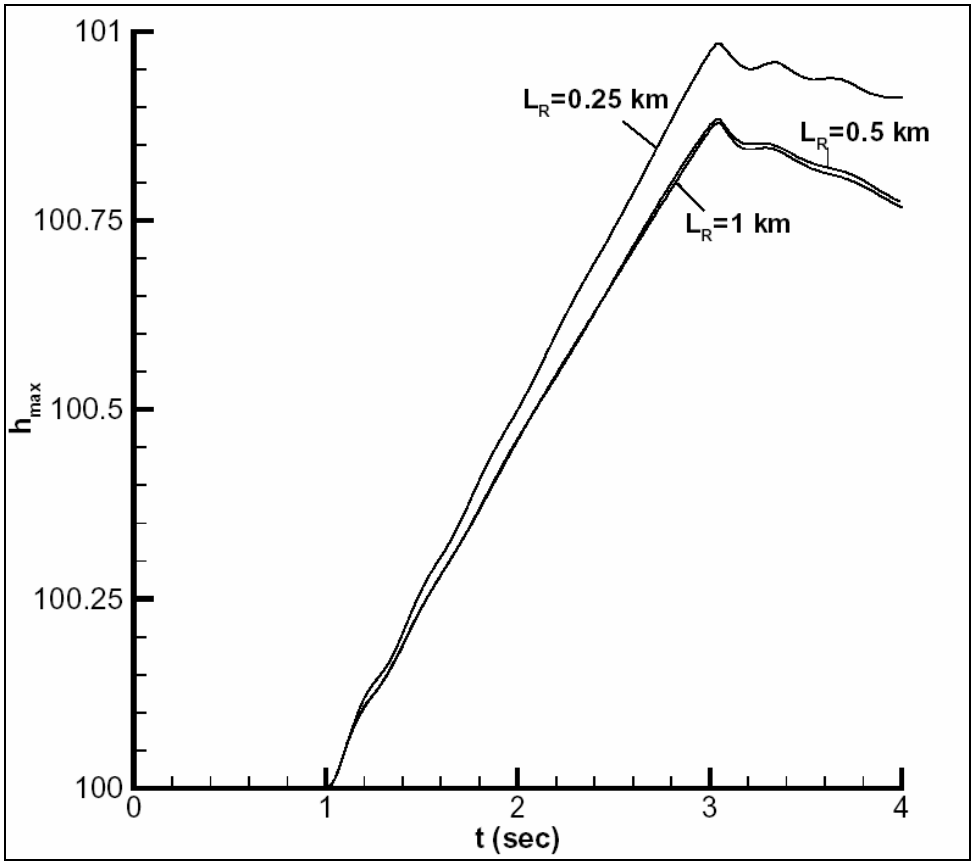

Figure 3.4 – Maximum water level on L_R alternatives for Case I

Free Surface Profiles and Pressure Fields:

The surface profiles for the Hypothetical Case I at different time instants are given in the following figures.

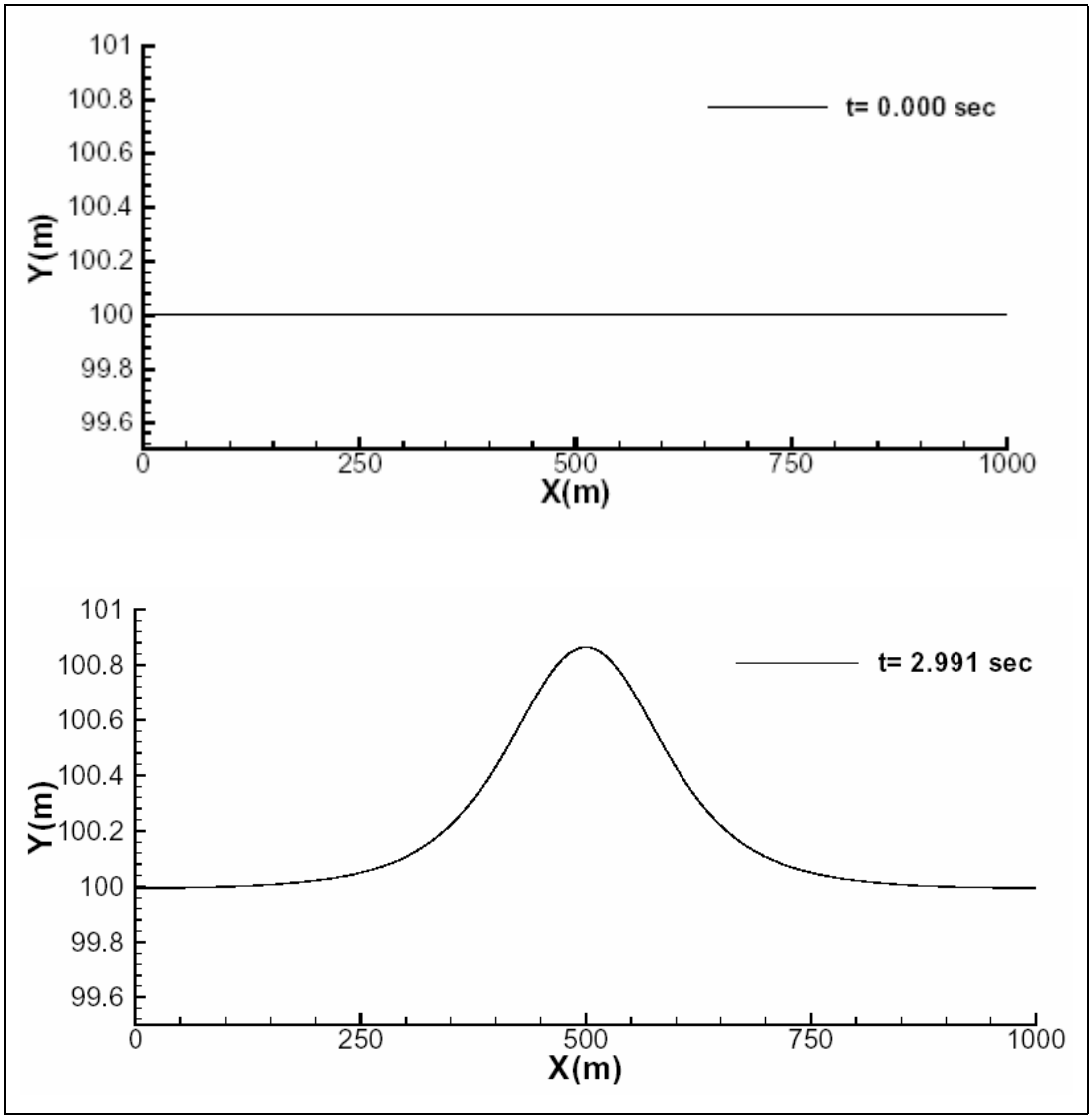

Figure 3.5 – Free surface profiles of Case I

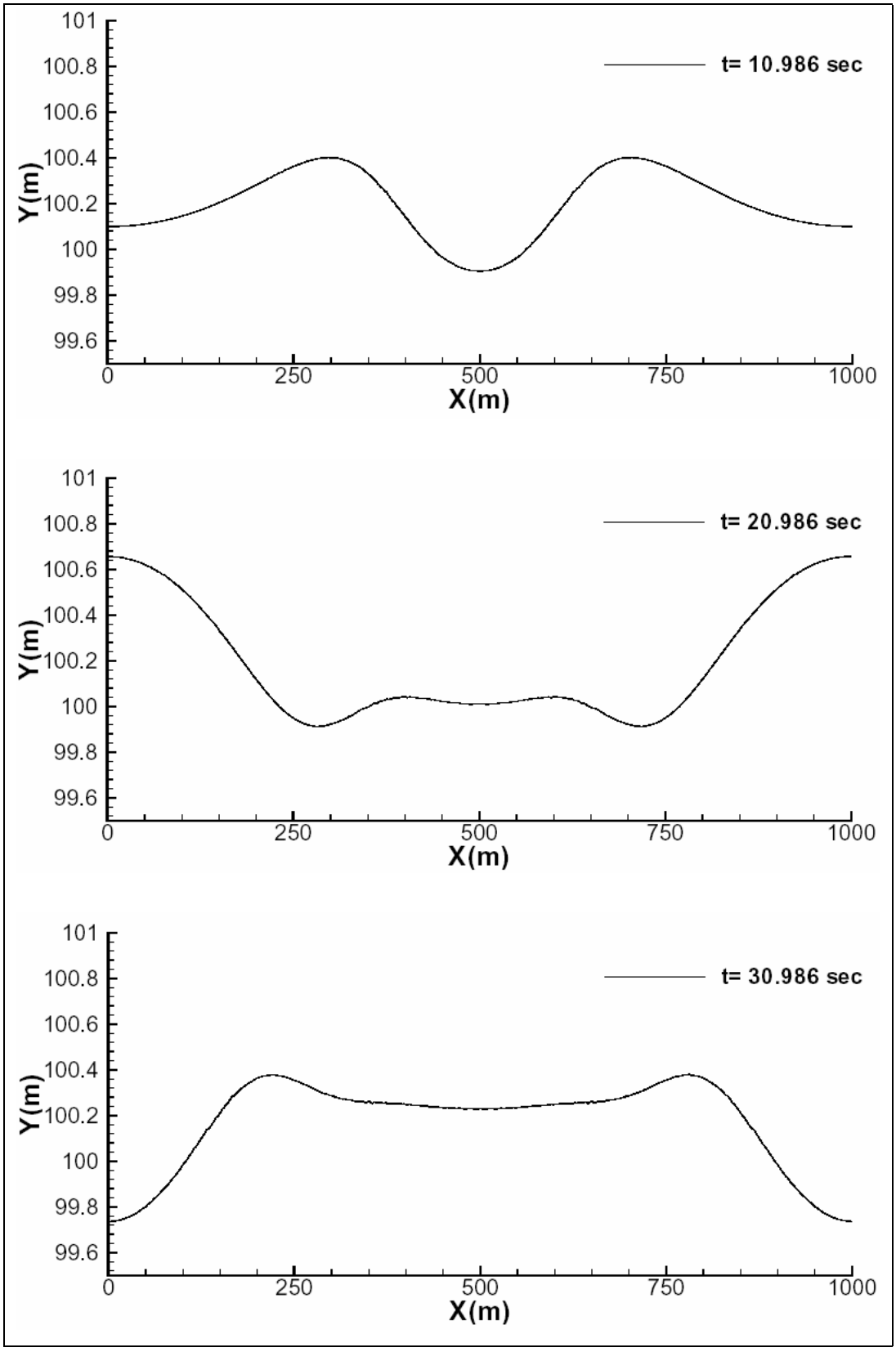

Figure 3.5 (continued) – Free surface profiles of Case I

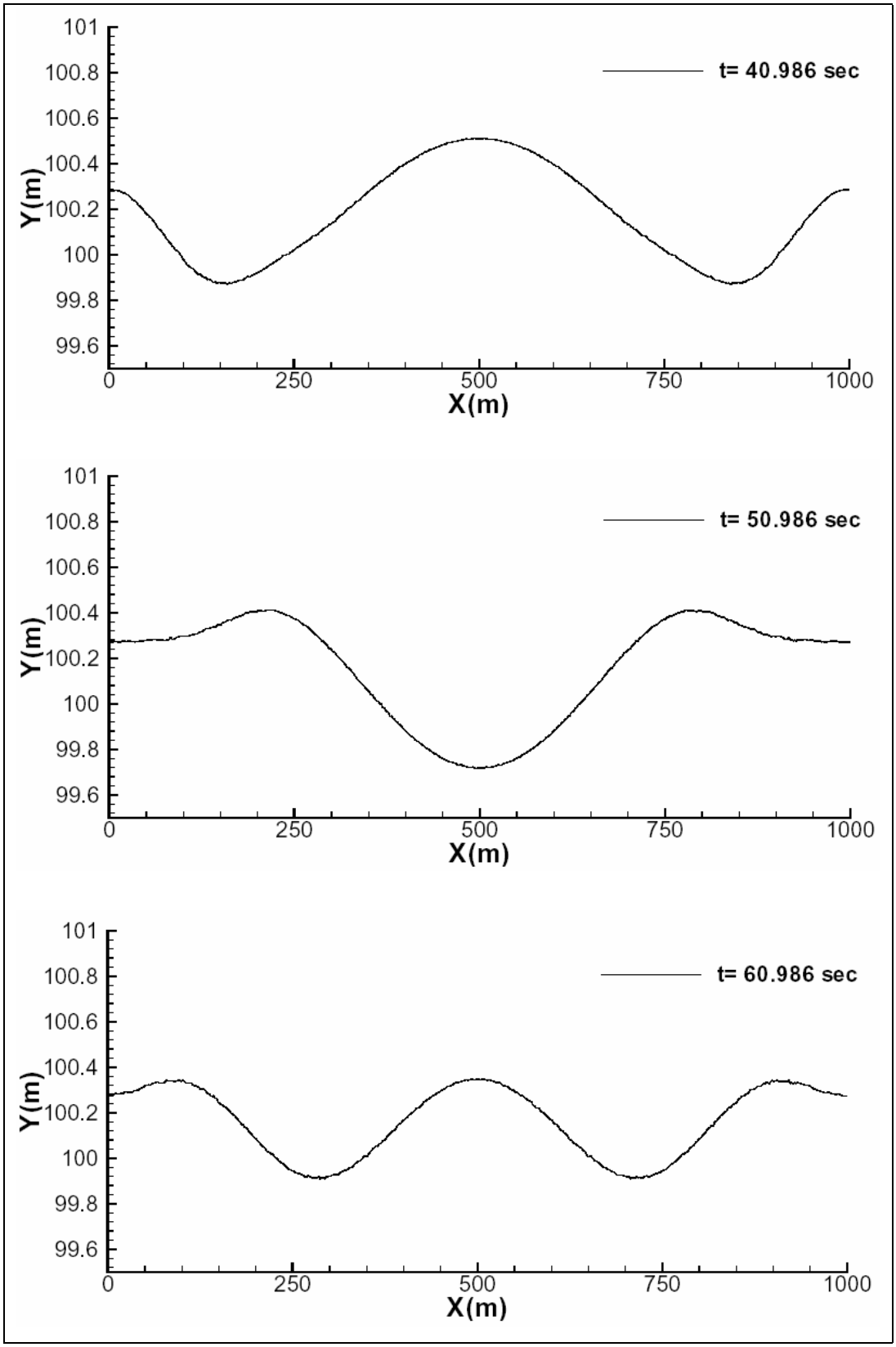

Figure 3.5 (continued) – Free surface profiles of Case I

The pressure fields at different time instants are given in the following figures.

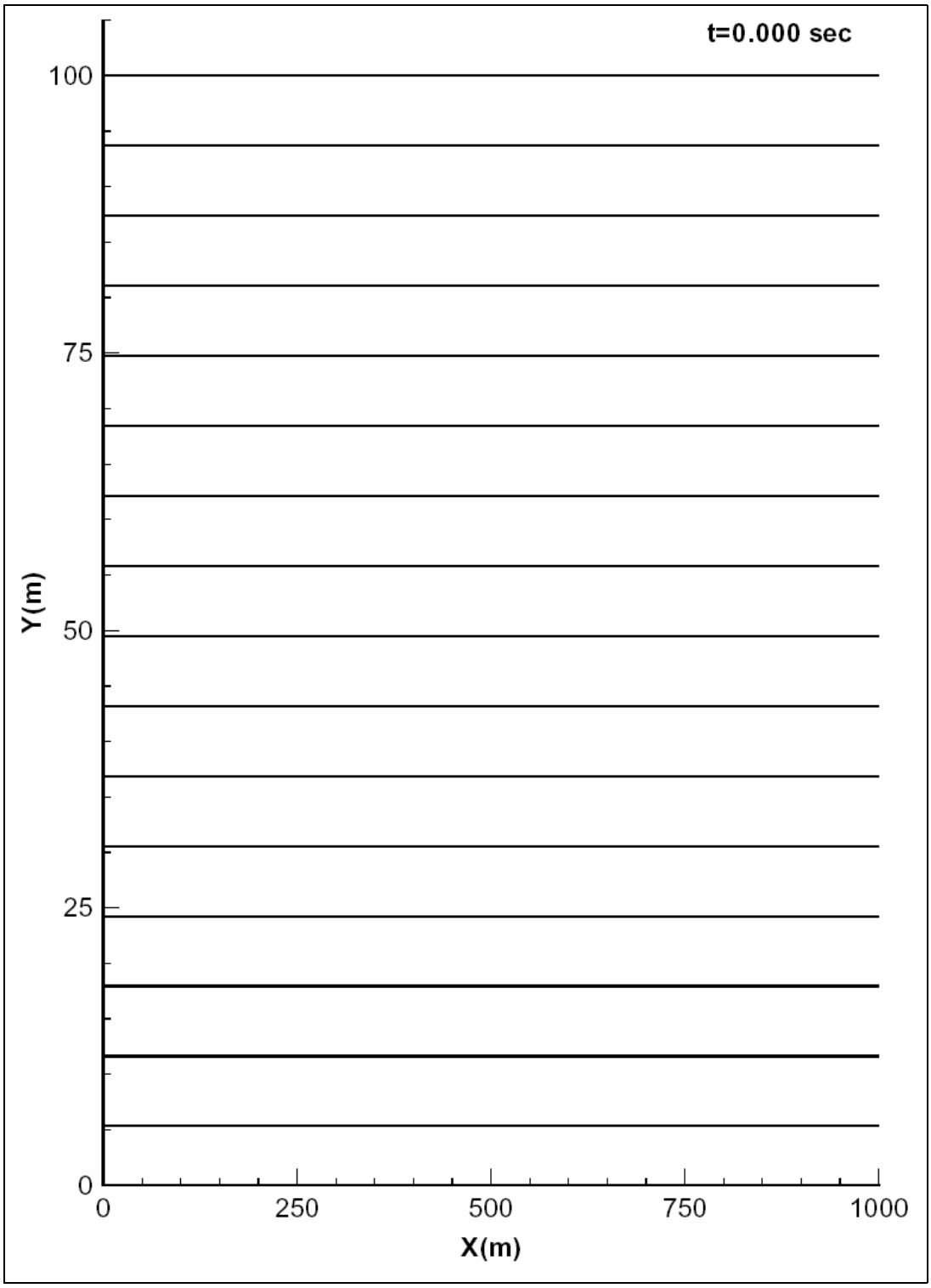

Figure 3.6 – Pressure fields of Case I

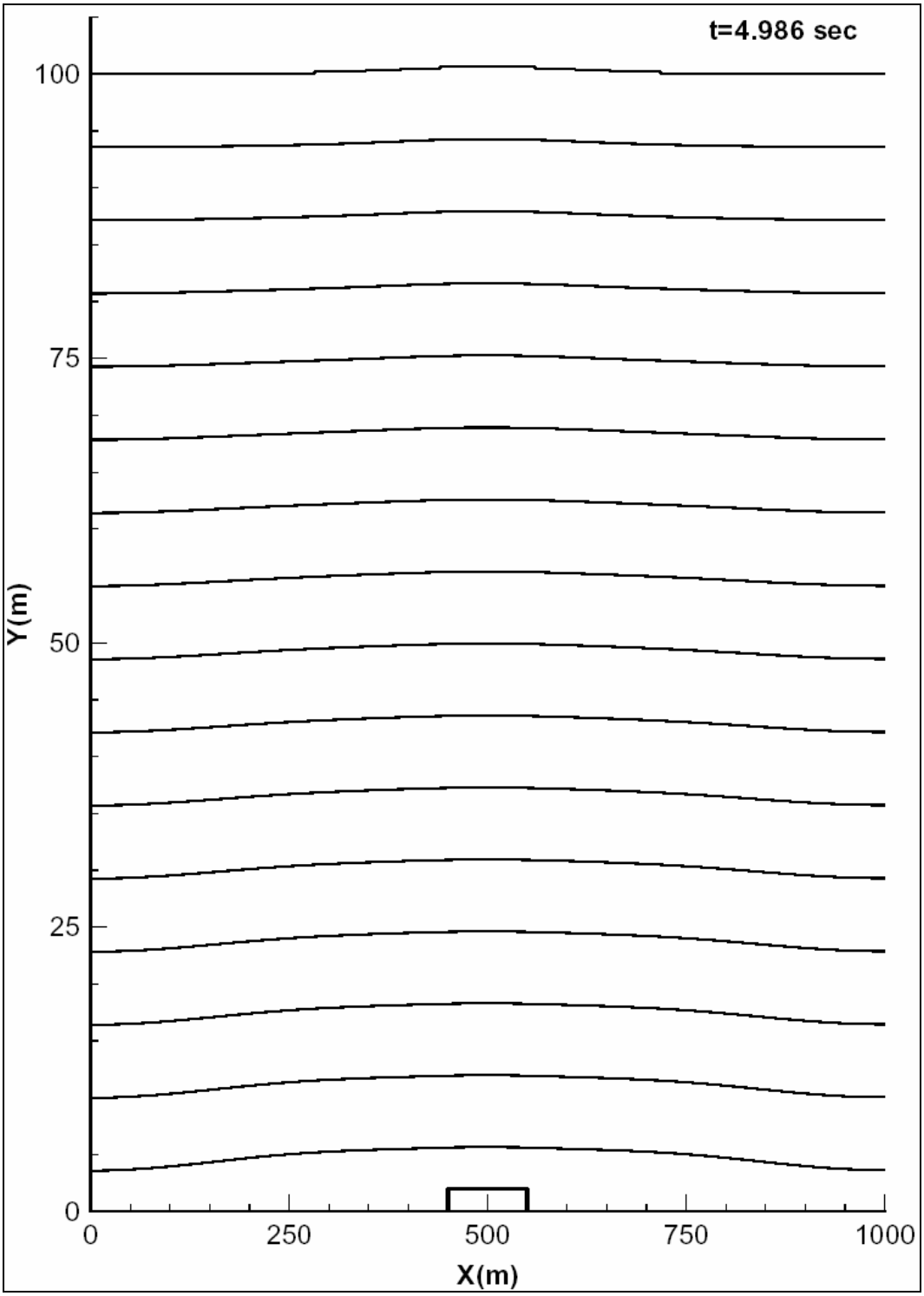

Figure 3.6 (continued) – Pressure fields of Case I

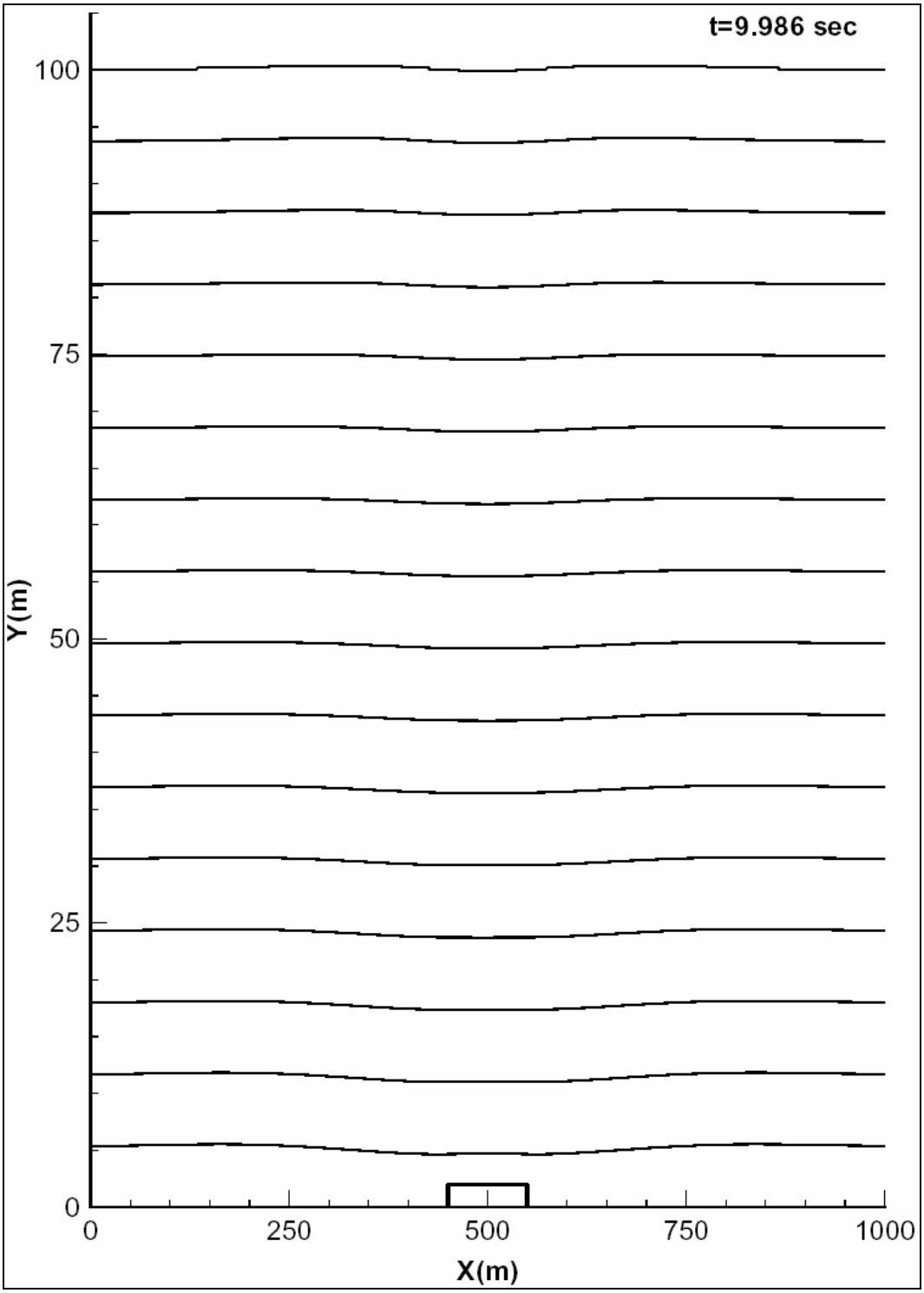

Figure 3.6 (continued) – Pressure fields of Case I

3.1.2 Hypothetical Case II (1 km depth)

The hypothetical reservoir is 10 km length (L_R) and the initial steady state hydrostatic water depth (H) is 1 km. At t=1 sec, subsidence volume (L_S=1 km) in the middle of the reservoir bed starts to move upwards in vertical direction with a constant velocity of 1 m/s. The motion continues until t=3 sec and this partial section of the reservoir bed rises 2 m in elevation.

Determination of optimum horizontal mesh:

The instantaneous volume/initial volume graphs for δx=20m (i_{max}=500), δx=50m (i_{max}=200) and δx=100m (i_{max}=100) alternatives on a vertical mesh parameters of δy_{min}=0.625 m, δy_{max}=4.15 m and j_{max}=500 are given below in Figure 3.7.

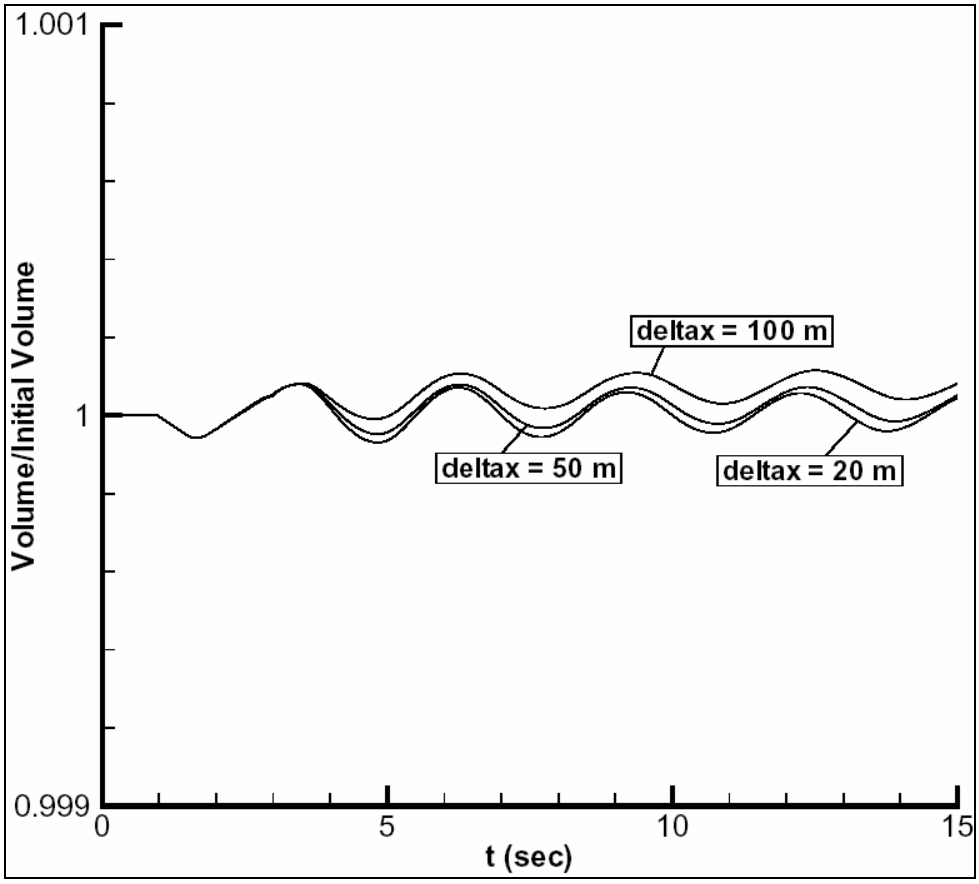

Figure 3.7 – Instantaneous volume/initial volume for Case II (using vertical mesh parameters of δy_{min}=0.625 m, δy_{max}=4.15 m and j_{max}=500)

From Figure 3.7 it is interpreted that on a coarse horizontal mesh size of δx=100m (i_{max}=100), the volume of the water has an increasing tendency, which is unphysical and unacceptable. However, for the finer meshes of δx=50m (i_{max}=200) and δx=20m (i_{max}=500) the volume changes are small and does not show an accumulating behavior and the divergence from unity is tolerable.

Figure 3.8 shows the maximum-recorded water height in the entire reservoir. From Figure 3.8 it is interpreted that as the horizontal mesh δx is refined the solution converges to a more accurate state. The graphs for δx=20m (i_{max}=500), δx=50m (i_{max}=200) are consistent in shape and small differences in values are tolerable.

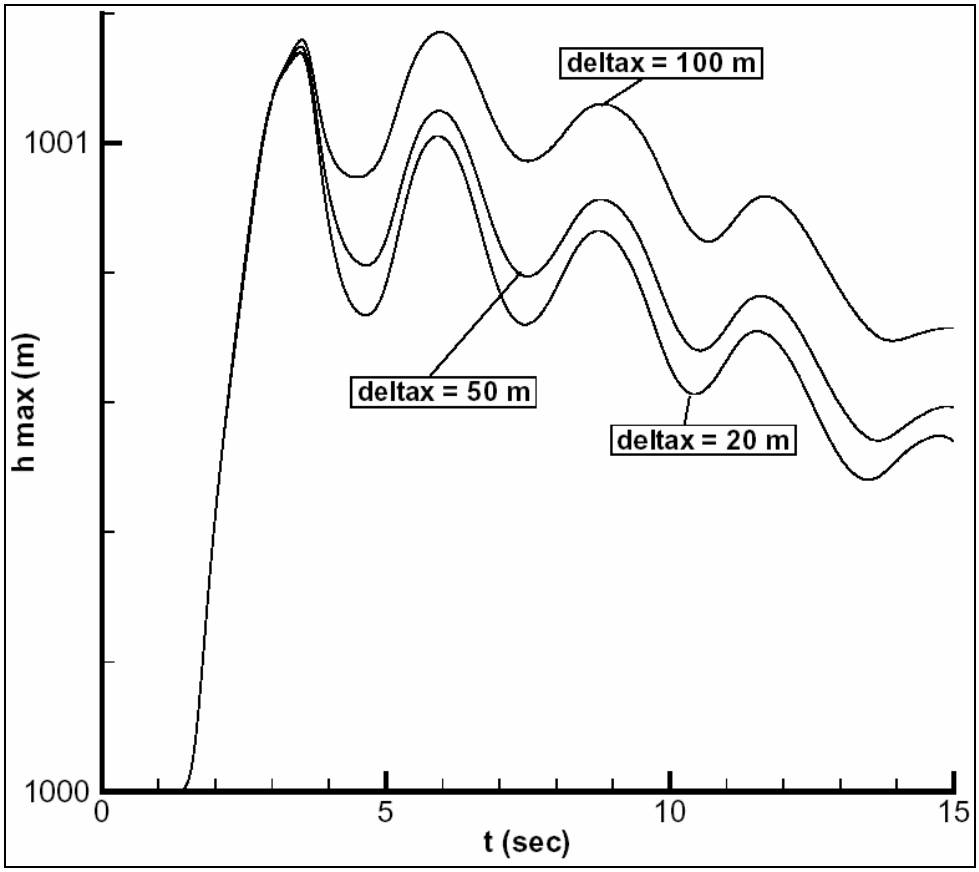

Figure 3.8 – Maximum water level on horizontal mesh alternatives for Case II (using vertical mesh parameters of δy_{min}=0.625 m, δy_{max}=4.15 m and j_{max}=500)

Determination of optimum vertical mesh:

The sufficiency of the vertical mesh used in the above tests is tested by solving the same problem using a two times finer vertical mesh. In the test the constant horizontal mesh size is taken as δx=20m (i_{max}=500).

The maximum-recorded water levels graph for the two vertical meshes is given in Figure 3.9.

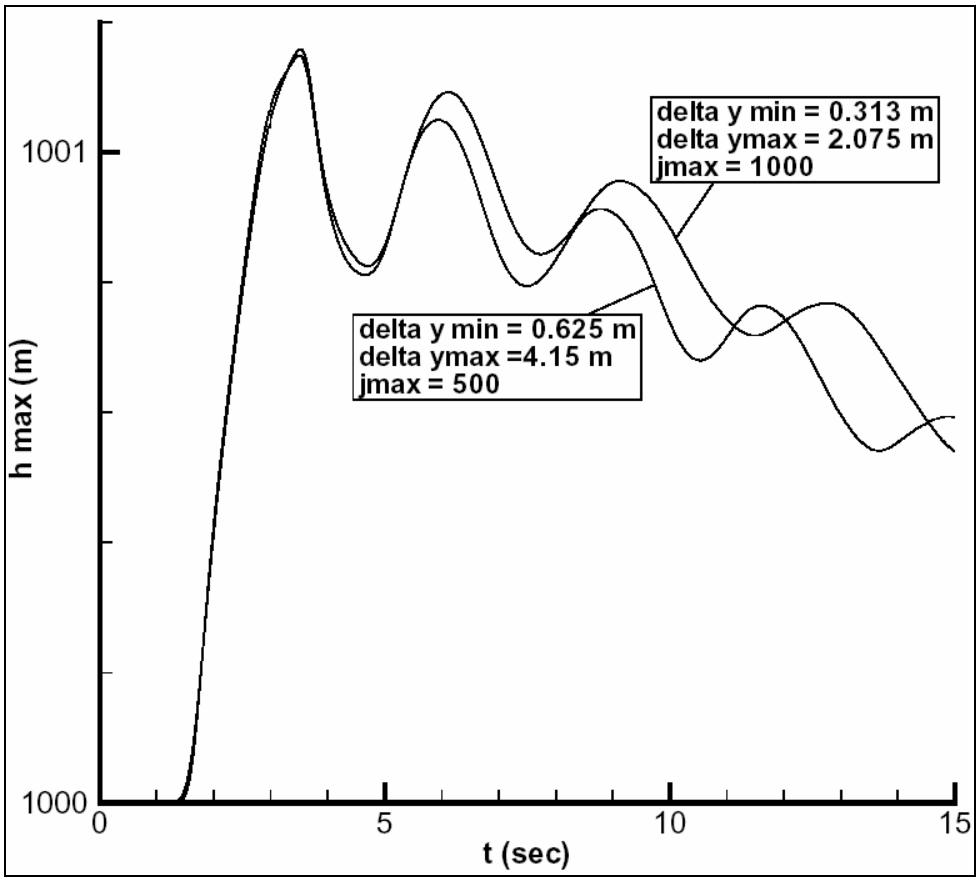

Figure 3.9 – Maximum water level on vertical mesh alternatives on δx=20m for Case II

The small differences in graphs given in Figure 3.9 are tolerable to prove the consistency of the results on the two different vertical mesh alternatives.

Finally, for the solution of Hypothetical Case II the computational mesh is set uniform in horizontal direction having a constant width δx=20m (i_{max}=500). In vertical direction (j_{max}=500), the mesh is set variable which gets finer near the free surface and at the reservoir bottom (δy_{min}=0.625m), and gets coarser in the interior regions (δy_{max}=4.15 m). Although this is not the best mesh alternative for a high precision solution, since the computation time on finer mesh alternatives is observed to be getting excessively long, for this demonstration case the mesh configuration is selected to be slightly coarse.

Verification of Reservoir Length and Side Boundary Conditions:

To check whether L_R = 10 km is sufficient, the same problem is solved for three L_R alternatives (Figure 3.10) and convergence at L_R = 10 km is verified.

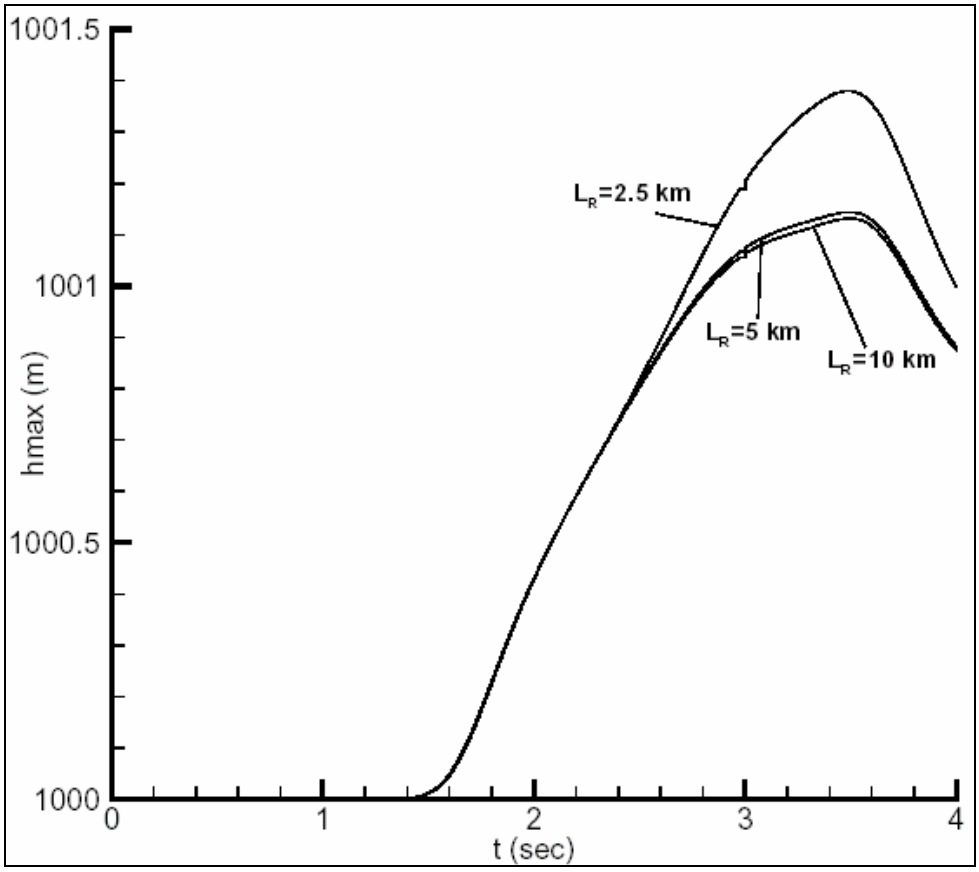

Figure 3.10 – Maximum water level on L_R alternatives for Case II

Free Surface Profiles and Pressure Fields:

The surface profiles for the Hypothetical Case II at different time instants are given in the following figures.

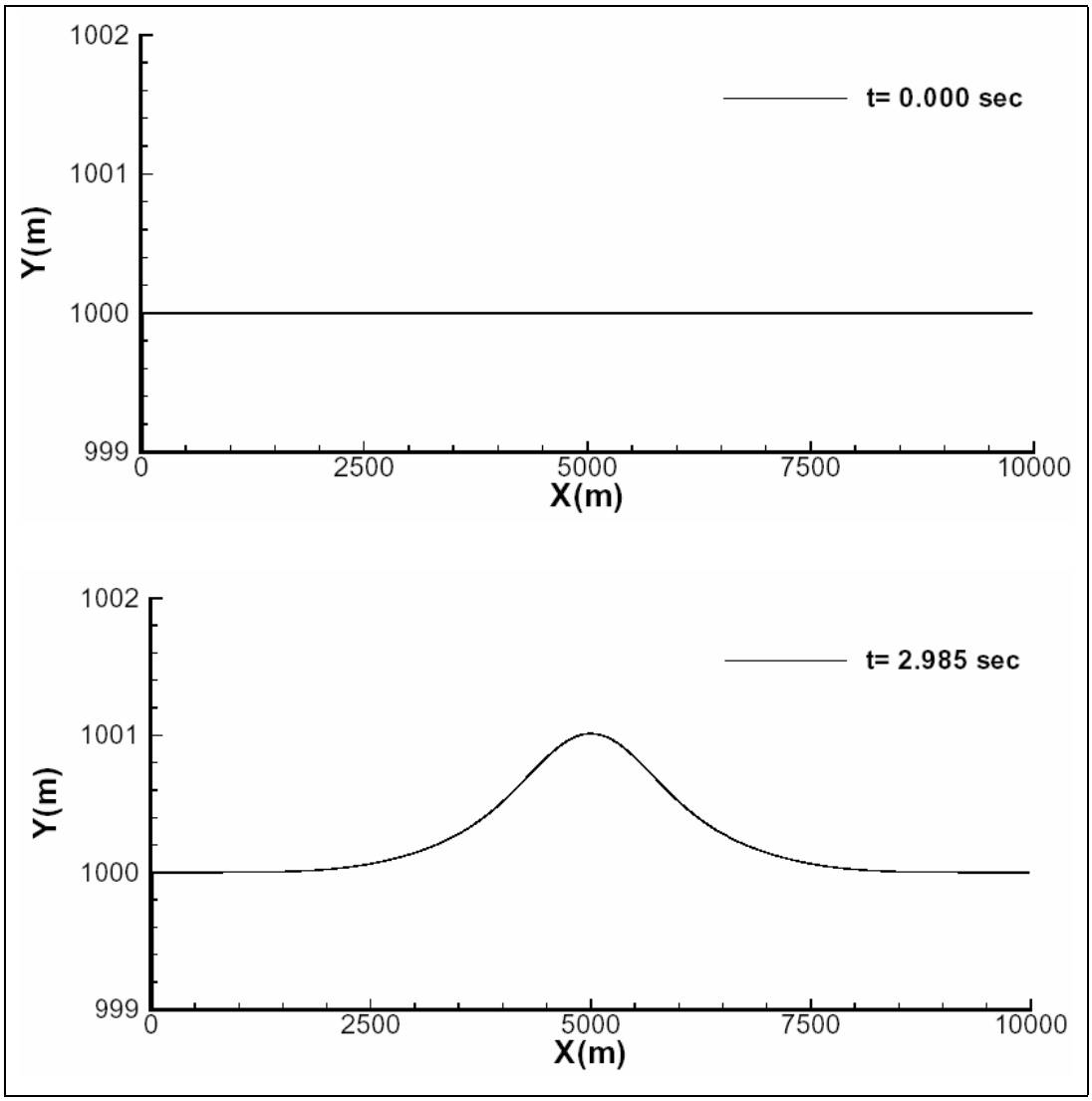

Figure 3.11 – Free surface profiles of Case II

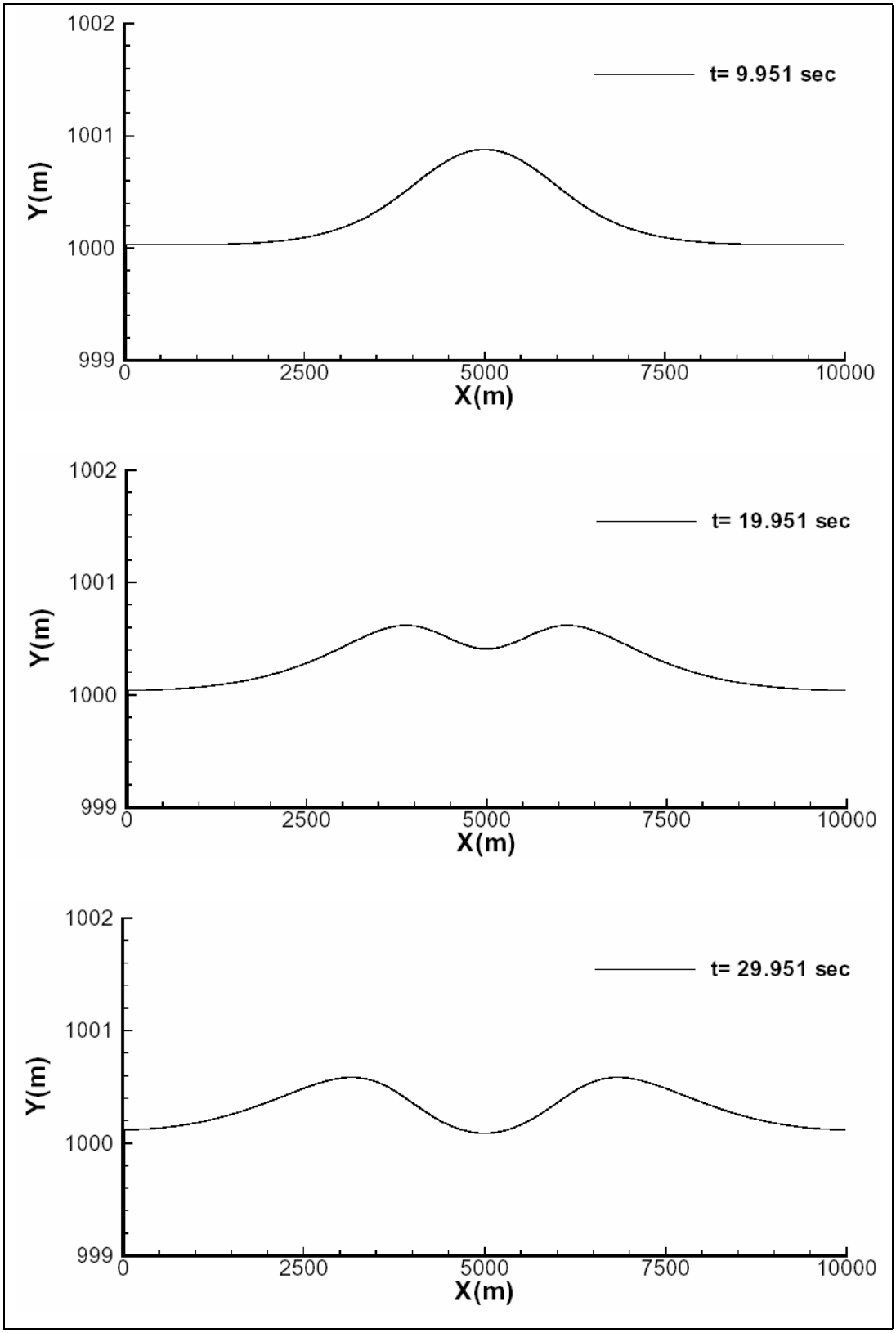

Figure 3.11 (continued) – Free surface profiles of Case II

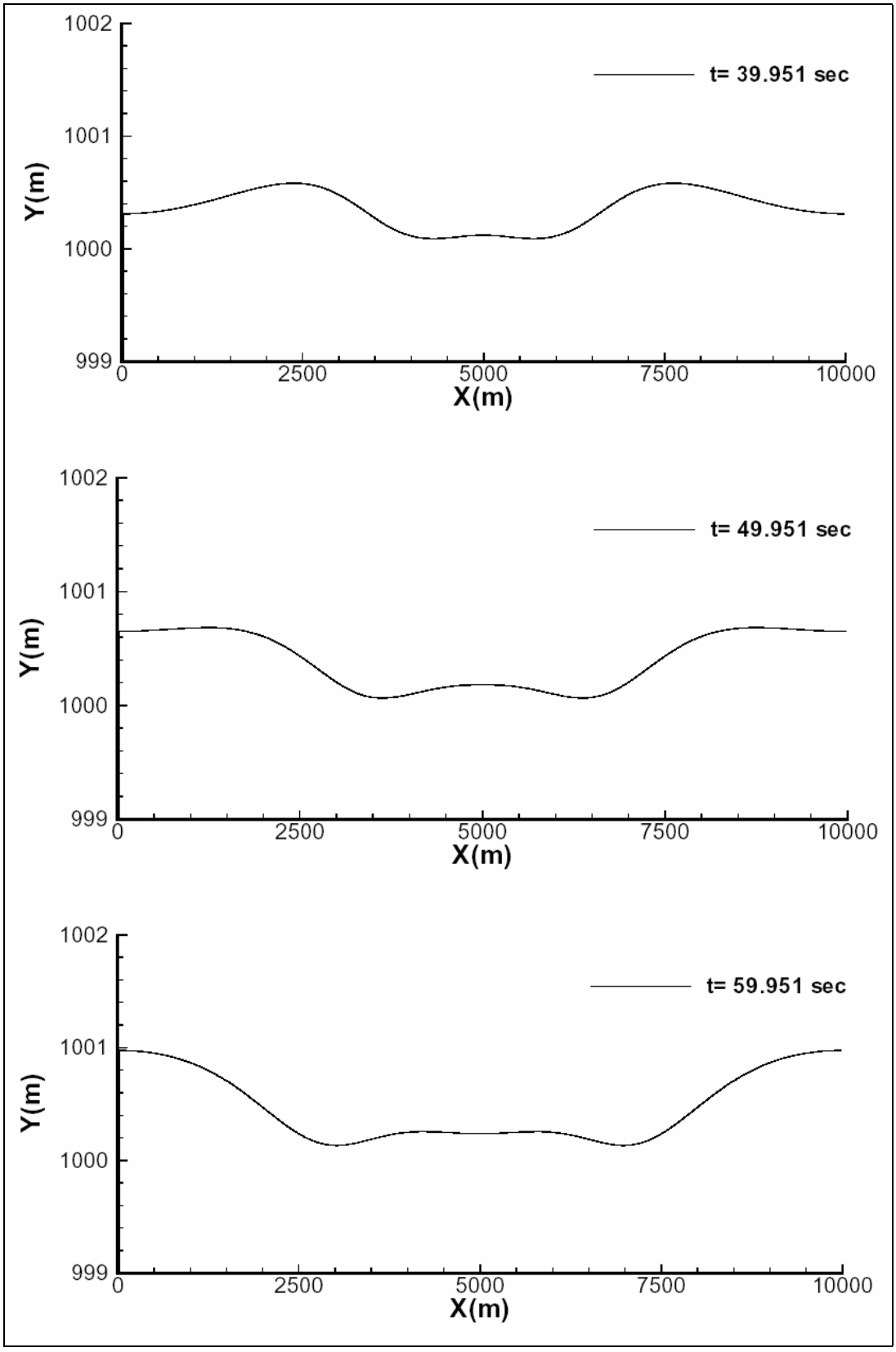

Figure 3.11 (continued) – Free surface profiles of Case II

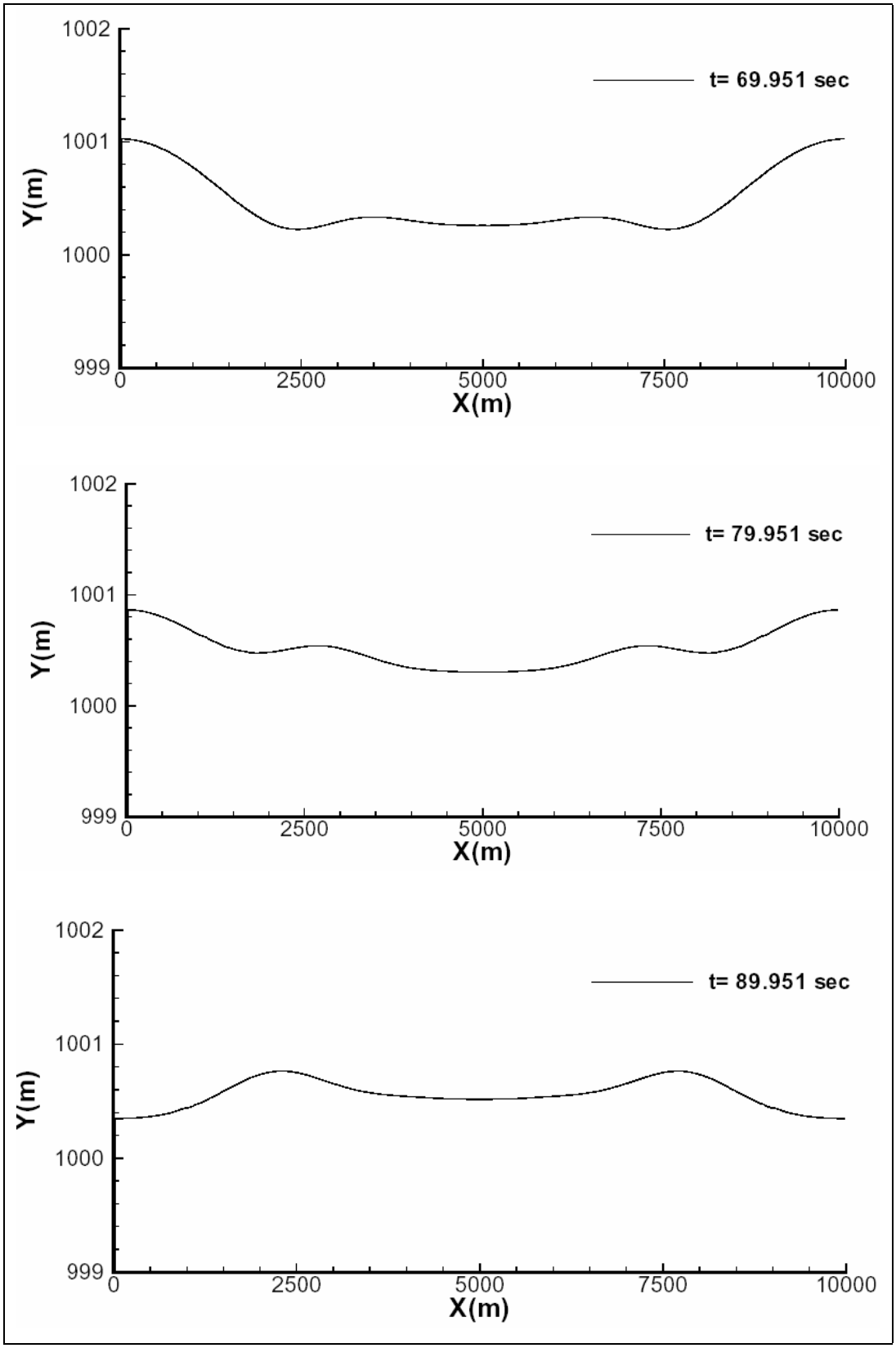

Figure 3.11 (continued) – Free surface profiles of Case II

The pressure fields at different time instants are given in the following figures.

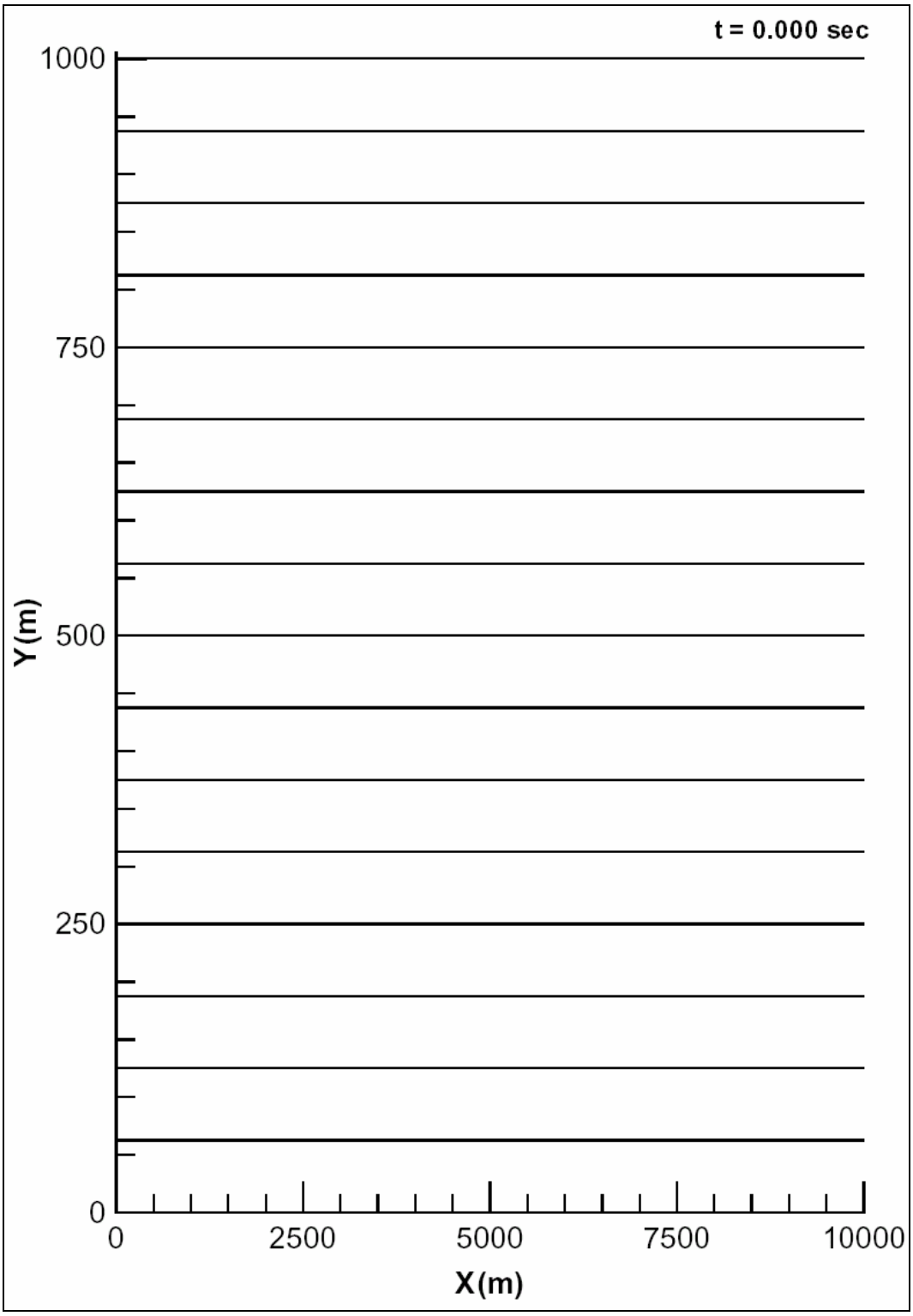

Figure 3.12 – Pressure fields of Case II

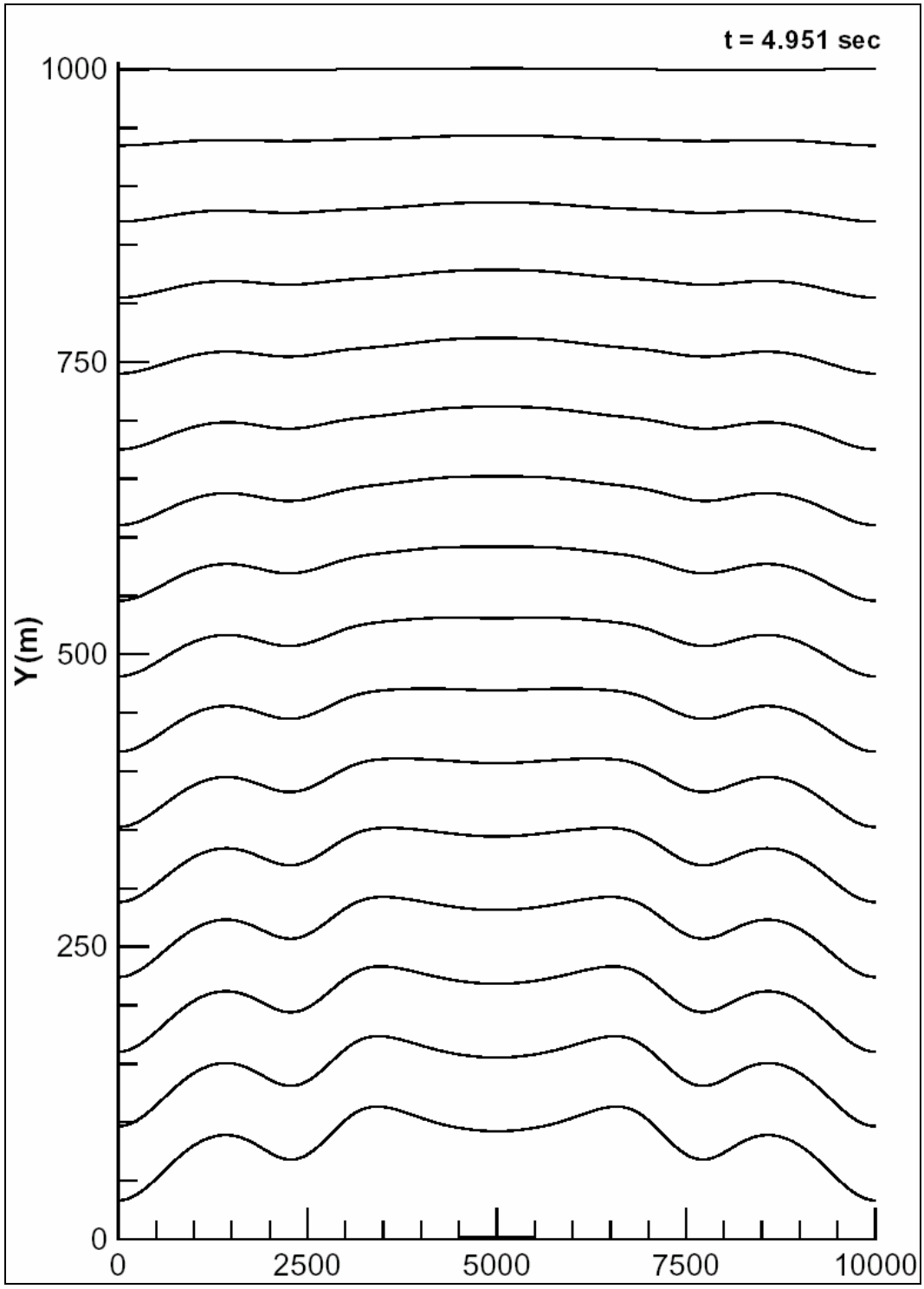

Figure 3.12 (continued) – Pressure fields of Case II

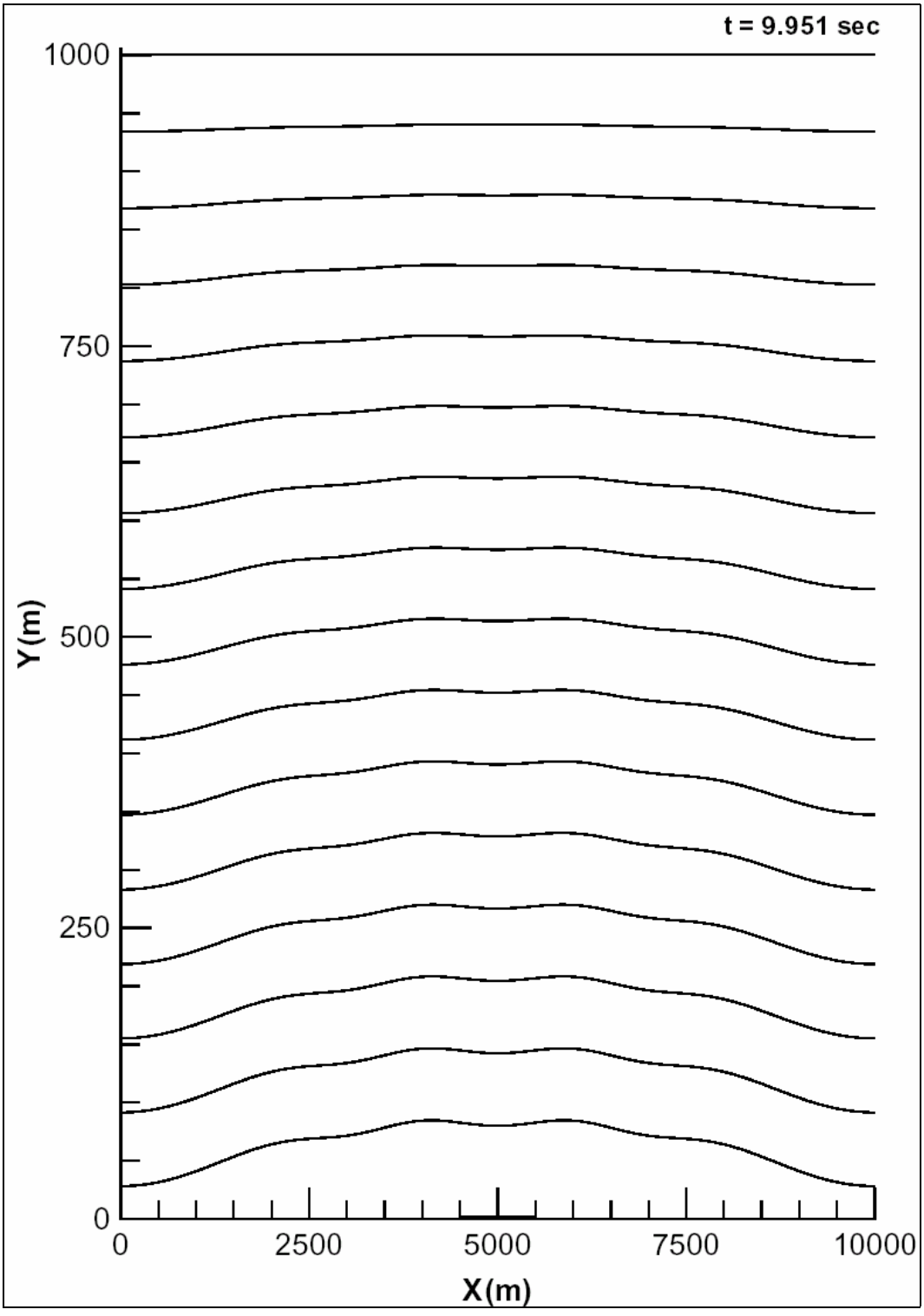

Figure 3.12 (continued) – Pressure fields of Case II

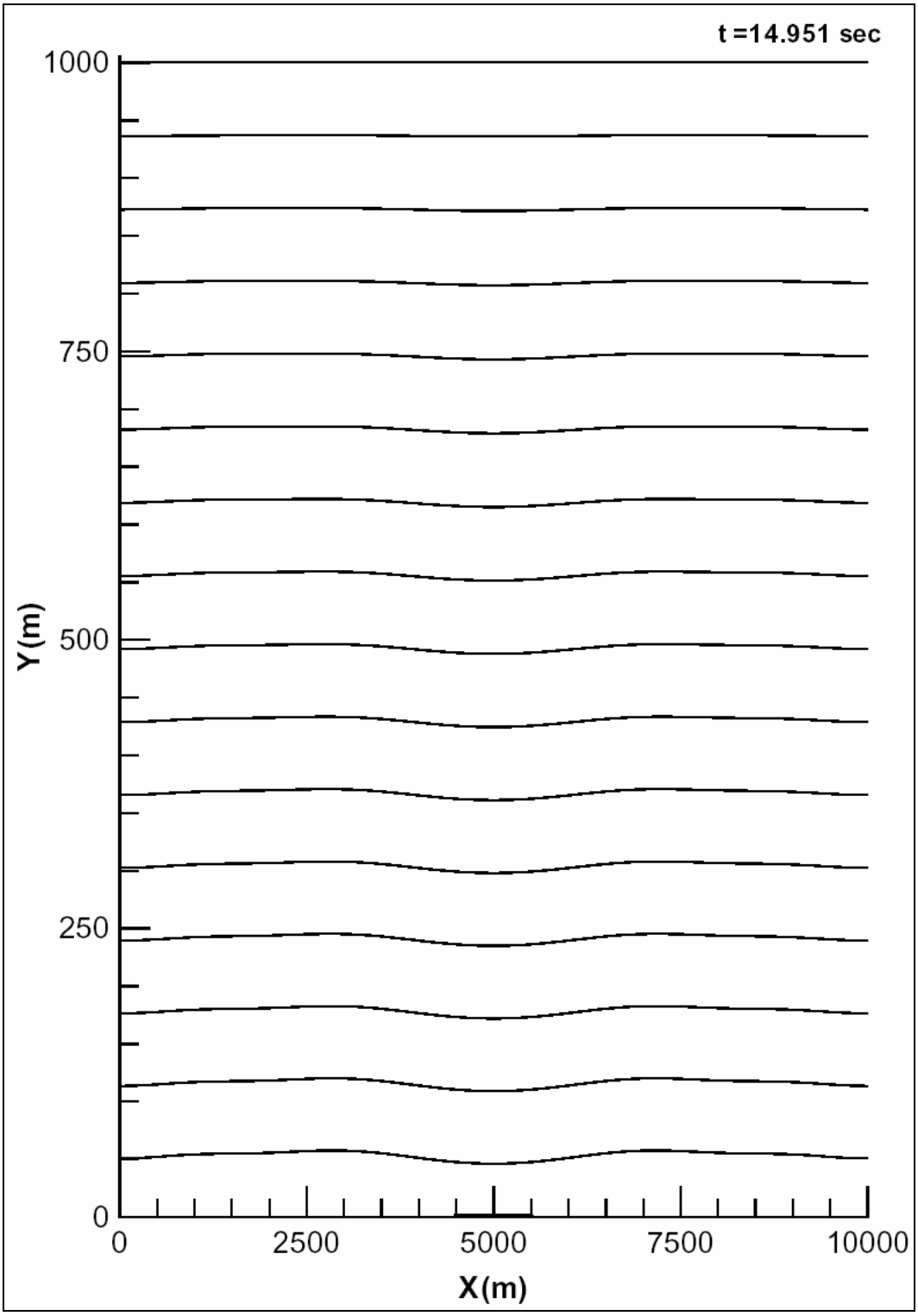

Figure 3.12 (continued) – Pressure fields of Case II

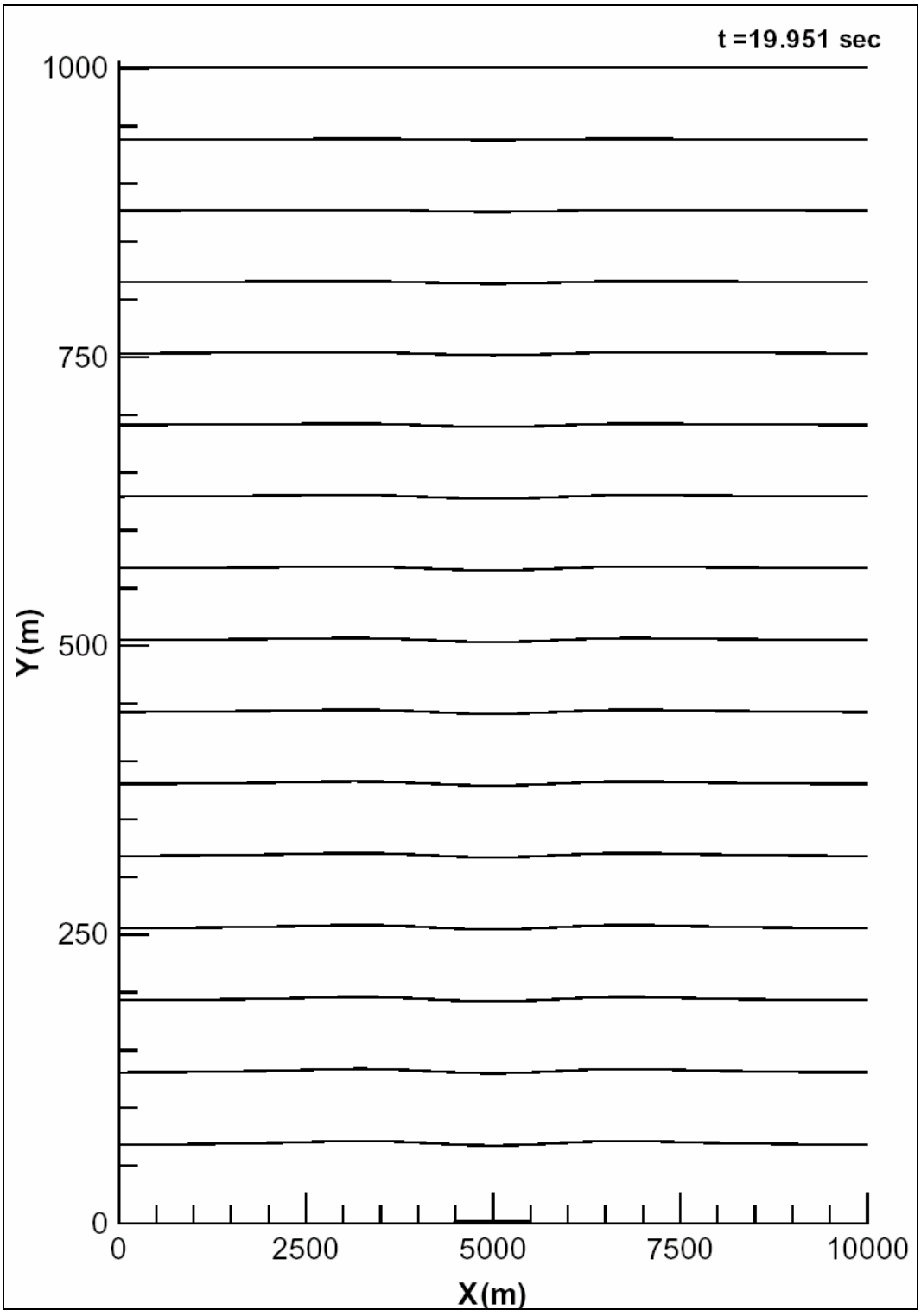

Figure 3.12 (continued) – Pressure fields of Case II

Supplementary investigations on Case II:

Besides the physical properties of water (density, speed of sound, and kinematic viscosity) and gravitational acceleration (g_y) the parameters which affect the solution are initial water depth (H), reservoir length (L_R), subsidence length (L_S), subsidence height (h_S) and subsidence velocity (V_S).

Under open sea conditions reservoir length (L_R) is large and it does not affect the solution. However, the effect of remaining parameters on the peak surface height can be investigated.

For H = 1 km, h_s = 2 m and V_s = 1 m/s the variation of peak surface height of water with respect to L_s is given in Figure 3.13.

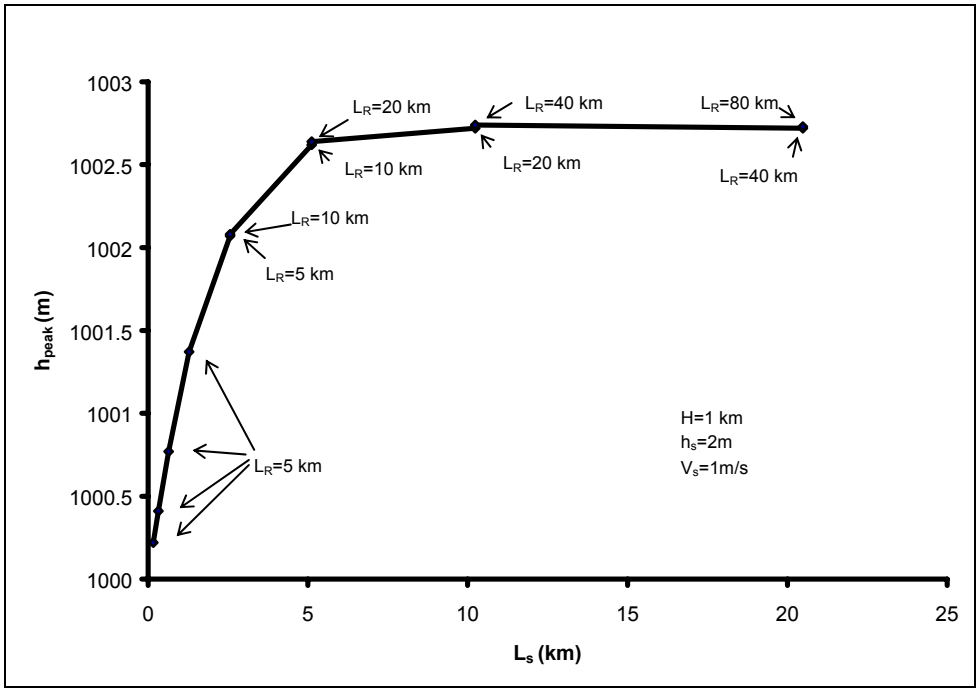

Figure 3.13 – Peak surface height vs L_s

From Figure 3.13 it is interpreted that, for this problem up to L_s=10 km (=10xH) there is dependence between L_s and the peak surface height of water. However after L_s=10 km (=10xH) the peak surface height of water does not

dependent of L_s. It is also shown on Figure 3.13 that, for this problem the open sea conditions are satisfied for L_R=2xL_S.

For H = 1 km, h_s = 2 m, L_R = 20 km and L_S = 10 km, the variation of peak surface height of water with respect to V_s is given in Figure 3.14.

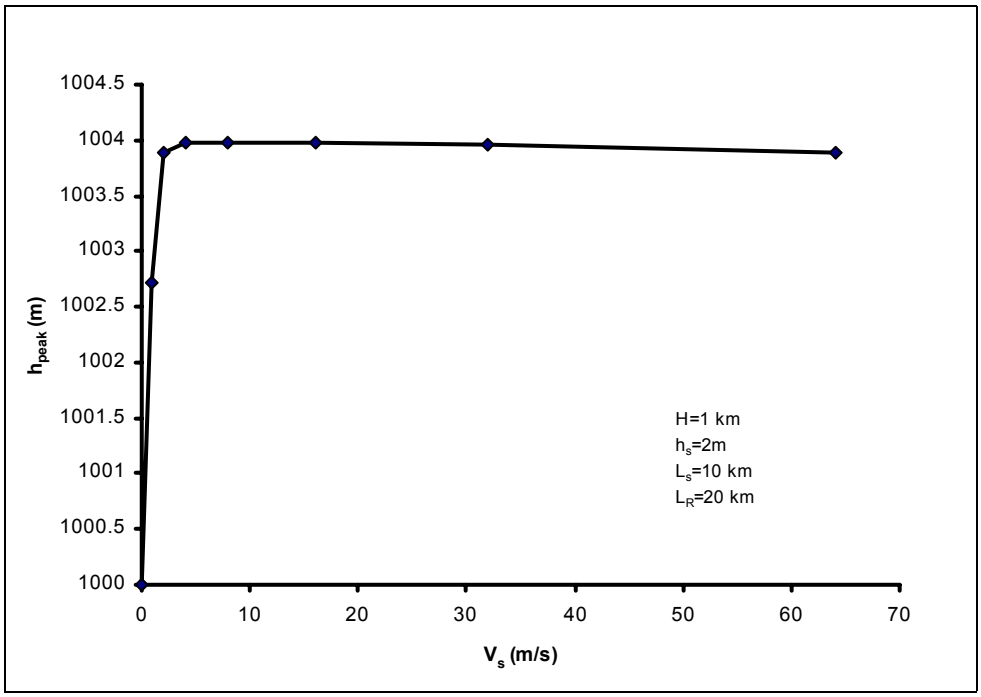

Figure 3.14 – Peak surface height vs V_s

From Figure 3.14 it is interpreted that, there is dependence between V_s and the peak surface height of water up to V_s = 8 m/s (≈0.08x$\sqrt{gH}$). However, for V_s>8 m/s the peak surface height of water does not depend on V_s.

It is also seen that the value of the peak surface height of water falls slightly when V_s takes large values (>30 m/s ≈ 0.02 x c). In the limited compressibility model the velocity of fluid is assumed to be small with respect to the speed of sound. As the velocity of fluid increases, the amount of error generated due to this assumption increases. The slight fall in the value of peak surface height is due to the error which becomes more significant as velocity increases.

3.2 Discussions on the Results

When the pressure contour plots of the two hypothetical cases are examined, the effect of the shock wave originating from the rapid ground motion can be observed. The contour lines, which were horizontal in the initial hydrostatic state, become curved upwards during the shock. The curvature is sharper near the shock area and it gets flattened away from the shock area.

It is also seen from the pressure contour plots that free surface is the last ring of the contour lines and the change in the free surface profile is a consequence of the change in profiles of the internal pressure contour lines.

When the contour plots of the pressure fields of the two hypothetical cases are compared, the curvature in the pressure field due to the shock is much sharper in the deeper case (Hypothetical Case II). This is because the effect of compressibility is more significant in deeper water volumes.

From the pressure contour plots, the vibrating motion within the entire reservoir can also be observed. This vibrating motion is similar to the harmonic motion of an elastic spring, which is observed after a given initial deformation.

As time passes, the kinetic energy of the fluid particles is transformed into heat by the action of molecular viscosity and the internal vibration of the reservoir is dumped.

As an observation, in the first 10-15 seconds of motion due to the vibrating motion described above the field parameters change rapidly in time. Thus the number of iterations for the convergence of PSOR iterative solution increases. Consequently the CPU time is long for the solution of the first 10-15 seconds of motion.

Although the vibrating motion within the reservoir water volume is dumped after a relatively short period of time, the free surface wave continues its motion without loosing much kinetic energy for a relatively long period of time.

3.3 Discussions on the Solution Method

The model computes the velocity and pressure field (u-v-p) for each of the computational cell within the entire reservoir volume. This time dependent computation procedure also involves an iterative solution of Poisson Equation for pressure parameter at every time step. The computer memory and processing facilities are exploited at full capacity during the computations. So it can be concluded that the model requires high capacity platforms for studying real-life problems.

The correct treatment of the free surface has been the major difficulty in this study. The first problem about the free surface was the tracking its correct location. In the early stages of this study marker particles were used to track the fluid cells. In this approach the free surface location was determined automatically according to the position of the marker particles. However, in the scope of this study highly complicated free surface deformations such as breaking of waves or formation of droplets are not observed and expected. So, it is not needed to solve such complicated surface problems.

In the later stages of this study Surface Height Method (Nichols and Hirt, 1973), described in section 2.6 was considered. This free surface tracking method fitted into the present model perfectly, since it uses minimum computer resources and gives sufficiently enough information about the location of the free surface.

The second problem about the free surface was application of the correct free surface boundary conditions. In the earlier stages of this study the pressure boundary condition of the free surface has been simply applied to the centers of surface cells. However, when the free surface profiles were examined unphysical oscillations had been observed at the time instants when the free surface moves from one cell to another.

In the later stages of this study the pressure boundary condition of the surface has been applied to its correct location using an interpolation scheme. This brought the advantage of sensing the motion of the free surface and applying the free surface boundary conditions more accurately. After this

modification the motion of the free surface between cells didn't create any unphysical jump in the field parameters and the unphysical oscillations observed on the free surface are removed.

In the scope of this study, instead of using the simple free surface boundary conditions of original MAC, which is correct only in limit of zero viscosity, the improved free surface conditions (Hirt and Shannon, 1968) were used. However, while deriving the free surface boundary conditions it is assumed that the free surface is nearly horizontal. This assumption is reasonable as far as the hypothetical cases (3.1.1 and 3.1.2) are considered since the wave height is very small compared to the wave length. However, the free surface boundary conditions can be improved to take care of the correct free surface slopes and water waves with steeper profiles.

Selection of the sufficiently fine mesh has been another critical task because of the two sensitive boundaries, i.e. the solid boundary in rapid motion and the free surface boundary in relatively free motion.

In the scope of this study the variations in the field parameters in horizontal direction were expected to be relatively small compared to the vertical direction. So no effort has been performed to modify the model to be able to work on variable horizontal meshes. However, during the study on hypothetical cases it was understood that a variable horizontal mesh would also be very useful when it is required to work on reservoirs which are very long in horizontal direction.

The model assumes irregular solid boundaries as full boundary cells. This brings a zigzag approximation to the sloping walls. The adverse affects of this approximation is not observed in the case problems since there were no sloping walls. However, the model can be upgraded to use better approximations near the irregular solid boundaries.

CHAPTER 4

CONCLUSIONS

A two-dimensional mathematical model has been developed for simulating generation of surface waves due to sudden movements at the sea bottom.

The model is applied to two hypothetical cases with the vertical ground displacement of 2m. The computed free surface profiles and the pressure fields at several time instants are presented.

The model successfully produced the time-dependent development of pressure waves and the surface waves. However, more detailed numerical analysis is required to discuss the physical aspects of the mathematical model.

Major conclusions of this study can be summarized as follows:

1. "Surface Height Method" is found to be an economical and appropriate method for surface profile tracking in large water volumes.

2. In the numerical solution, the vertical plane must be divided into three zones; the bottom layer, the surface layer and the main water volume in between. Grid clustering is required in the bottom and surface layers to achieve satisfactory accuracy.

3. In a reservoir, which has got a depth of 1 km, the length of the subsidence volume (L_S) should be greater than 5 km to get wave heights independent of L_S.

4. Reservoir length (L_R) should be at least $2xL_S$, to obtain surface waves, which are formed independent of the vertical side boundaries.

5. Speed of subsidence volume (V_S) must be above 8 m/s to observe the heighest possible wave formations on the free surface.

For further improvement of the model the following recommendations are made:

1. Grid clustering in horizontal direction must be considered.

2. The free surface boundary conditions can be improved by including the actual slope of the free surface.

3. The zigzag treatment of the irregular solid boundary geometries can be improved.

4. The program can be modified to work on higher capacity platforms (parallel computing facilities).

REFERENCES

Altinok, Y., Ersoy, S., Yalciner, A. C., Alpar, B., Kuran, U. 2001. Historical Tsunamis in the Sea of Marmara. ITS 2001 Proceedings, Session 4, Number 4-2: 527-534. Available from http://www.pmel.noaa.gov/its2001/Separate_Papers/4-02_Altinok.pdf

Chan, R. K.-C., Street R. L. 1970. A Computer Study of Finite-Amplitude Water Waves. *J. Comput. Phys.*, 6: 68-94.

Daly, B. J. 1969. A Technique for Including Surface Tension Effects in Hydrodynamic Calculations. *J. Comput. Phys.,*4: 97-117.

George P. C. 1999. Preliminary Report on The Earthquake and Tsunami of August 17, 1999 in Turkey. Initial bulletin August 23, 1999 - Further modified and updated on Aug 25 & Sept. 2 , 1999. Internet. Available from http://www.drgeorgepc.com/Tsunami1999Turkey.html

Griebel, M., Dornseifer, T. and Neunhoeffer, T. 1998. Numerical Simulation in Fluid Dynamics : A Practical Introduction. Society for Industrial and Applied Mathematics.

Harlow, F. H., Shannon, J. P. 1967. The Splash of a Liquid Drop. *J. Appl. Phys.*, 38: 3855-3866.

Harlow, F. H., Welch, J. E. 1965. Numerical Calculation of Time-Dependent Viscous Incompressible Flow of Fluid with Free Surface. *Phys. Fluids*, 8: 2182-2189.

Harlow, F. H., Welch, J. E. 1966. Numerical Study of Large-Amplitude Free-Surface Motions. *Phys. Fluids*, 9: 842-851.

Hirt, C. W. 1968. Heuristic Stability Theory for Finite Difference Equations. *J. Comput. Phys.*, 2: 339-355.

Hirt, C. W., Amsden, A. A., Cook J. L. 1974. An Arbitrary Lagrangian-Eulerian Computing Method for All Flow Speeds. *J. Comput. Phys.*, 14: 227-253.

Hirt, C. W., Cook, J. L. 1972. Calculating Three-Dimensional Flows around Structures and over Rough Terrain. *J. Comput. Phys.*, 10: 324-340.

Hirt, C. W., Nichols, B. D. 1980. Adding Limited Compressibility to Incompressible Hydrocodes. *J. Comput. Phys.,* 34: 390-400.

Hirt, C. W., Nichols, B. D. 1981. Volume of Fluid (VOF) Method for the Dynamics of Free Boundaries. *J. Comput. Phys.,* 39: 201-225.

Hirt, C. W., Shannon, J. P. 1968. Free-Surface Stress Conditions for Incompressible – Flow Calculations. *J. Comput. Phys.*, 2: 403-411.

Flow Science Inc. Free Surface Modeling Methods. Internet. Available from http://www.flow3d.com/Cfd-101/freesmod.htm

NaSt2D. ftp://ftp.lrz-muenchen.de/pub/science/fluiddynamics/cfd/NaSt2D/

Nichols, B. D., Hirt C. W. 1971. Improved Free Surface Boundary Conditions for Numerical Incompressible-Flow Calculations. *J. Comput. Phys.*, 8: 434-448.

Nichols, B. D., Hirt C. W. 1973. Calculating Three-Dimensional Free Surface Flows in the Vicinity of Submerged and Exposed Structures. *J. Comput. Phys.*, 12: 234-246.

Streeter, V. L. 1961. Handbook of Fluid Dynamics. McGraw-Hill Book Company, Inc.

Viecelli, J. A. 1969. A Method for Including Arbitrary External Boundaries in the MAC Incompressible Fluid Computing Technique. *J. Comput. Phys.* 4: 543-551.

Viecelli, J. A. 1971. A Computing Method for Incompressible Flows Bounded by Moving Walls. J. Comput. Phys., 8: 119-143.